[redacted]

UNCLASSIFIED

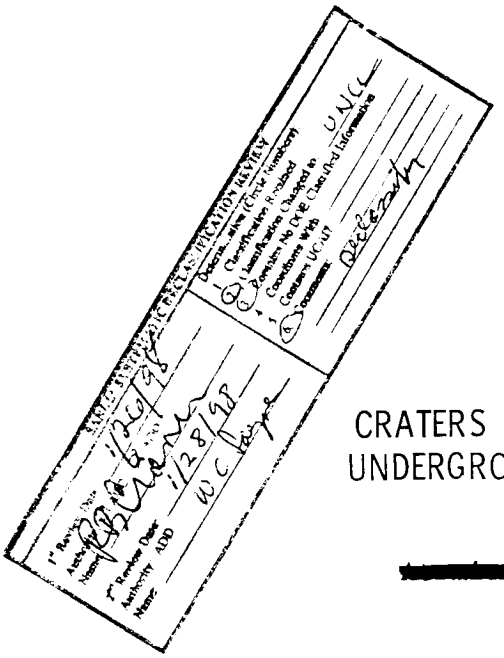

SANDIA SYSTEMATIC DECLASSIFICATION REVIEW
DOWNGRADING OR DECLASSIFICATION STAMP

CLASSIFICATION CHANGED TO: U AUTHORITY: W C Layne
Emelda Selph 2/3/98
PERSON CHANGING MARKING & DATE: LB Cramer 2/3/98 RECORD ID: 98SN1501
PERSON VERIFYING MARKING & DATE: DATED: 2/2/98

SC-RR-68-140 (Vol. 1)

CRATERS AND CAVITIES FORMED BY UNDERGROUND NUCLEAR EXPLOSIONS VOLUME I (U)

[redacted]

W. W. Hakala
Civil Engineering Department
University of New Mexico

ABSTRACT (U)

A study was made of cavities and subsidence craters formed as a result of contained nuclear explosions. From tests on similar geologic materials, it was found that measured cavity radius scales as the 1/3 power of the yield. Studies of subsidence-crater volumes indicated that the measured cavity radius is not always an indicator of true cavity geometry. The geometry of the subsidence crater is dependent upon the scaled burial depth, while collapse time is strongly influenced by the strength characteristics of the geologic medium. A bulking theory is proposed to determine subsidence-crater values from a known yield and depth of burial. Inversely, the yield may be estimated from the subsidence-crater parameters by using empirical equations. It appears essential to relate the physical properties of the medium to the measured values of cavities and craters in order to reduce scatter in the data. The largest yield considered in these analyses was 124 kt at 1622 feet; the deepest shot considered was 100 kt at 1768 feet.

[redacted]

September 1968

jr

UNCLASSIFIED

[redacted]

ACKNOWLEDGMENT

These experiments were conducted as part of the Plowshare program for the Atomic Energy Commission.

The work reported here was done at Sandia Corporation, Albuquerque, New Mexico, in the Underground Physics Division (M. L. Merritt, Supervisor), under an Associated Rocky Mountain Universities (ARMU) summer faculty orientation grant. The author wishes to express his gratitude to Mr. L. J. Vortman of Sandia for his helpful suggestions and valuable guidance in preparation of the report. Appreciation is also expressed to Mr. Gilbert E. Larsen, also of Sandia, who did the programming for the computer calculations.

Numerous people contributed to the yield, cavity, and crater data reported here, including Charles I. Browne, Jr., Rea Blossom, and Robert J. Bradshaw, LASL; A. F. Clark and Donald E. Rawson, LRL; and personnel of Holmes and Narver, Inc., American Aerial Surveys, Inc., and Limbaugh Engineers, Inc.

Printed in the United States of America
Available from
Clearinghouse for Federal Scientific and Technical Information
National Bureau of Standards, U. S. Department of Commerce
Springfield, Virginia 22151
Price: Printed Copy $3.00; Microfiche $0.65

FOREWORD

This is Volume I of a three-volume work. Volume I contains the text; Volume II contains the classified information on which the text is based; and Volume III contains unclassified contour maps of the subsidence craters. The bibliographical information is as follows:

SC-RR-68-140 (Vol. I) - Craters and Cavities Formed by Underground Nuclear Explosions

SC-RR-68-141 (Vol. II) - Craters and Cavities Formed by Underground Nuclear Explosions: Index of Events and Classified Contour Maps

SC-RR-68-142 (Vol. III) - Craters and Cavities Formed by Underground Nuclear Explosions: Unclassified Contour Maps

[redacted]

CONTENTS

[redacted]

SYMBOLS

A - alluvium

B - bulking factor

C - material constant

$\overline{C}$ - average C

DOB - depth of burial

E - energy of explosive charge

G - compressibility of geologic medium

GZ - ground zero

K - coefficient of lateral earth pressure

K_i - constant

L - lower limit of DOB/R for an ejection crater

M - mass

R - cavity radius

S_f - critical stress in wall of cavity

T - tuff

V - volume

V_c - volume of cavity

V_s - volume of subsidence crater

W - mass of nuclear charge

WP - working point

a - radius of subsidence crater

b - thickness of assumed cavity wall

c - sonic velocity, cohesion of soil

d_c - height of chimney

e - distance from center of nuclear charge

f_i - function

g - gravitational constant

h - depth of crater

i - pressure gradient

k - coefficient of permeability

m - constant depending on crater profile

n - porosity of soil

p - gas pressure

p_f - gas pressure at initial collapse

r - radius

r_f - radius at initial collapse

t - time

t_c - total collapse time

t_f - time at initial collapse

v - velocity

w - unit weight of soil ($w = \rho g$)

z - distance below surface

α, β - constants

γ - gas constant

π - Pi

ρ - mass density

σ_H - lateral earth pressure

σ_v - vertical earth pressure

ϕ - angle of internal friction of soil

θ - angle between vertical and failure surface above cavity

CRATERS AND CAVITIES FORMED BY UNDERGROUND NUCLEAR EXPLOSIONS

CHAPTER I

Introduction and Summary

With the rapidly expanding possibilities for engineering applications of nuclear explosives, it is necessary to have a thorough understanding of the physical effects of a nuclear blast. In this report, certain aspects of a contained nuclear explosion are considered; namely, the size of the cavity formed about a nuclear source, and the dimensions of the subsidence crater formed at the surface.

Uses of cavity and crater volumes play an important part in the Plowshare program. Some applications of contained nuclear explosions presently being considered are: creating of underground reservoirs for storage purposes; fracturing of oil shale to increase production; crushing of underground ores to facilitate mining; increasing the capacity of water-bearing aquifers, and producing of chemicals.

At first glance, it would appear that subsidence craters resulting from a contained explosion would not have great value, especially since much greater efficiency of cratering is obtained by placing the explosive at optimum depth. However, when it is mandatory to contain radioactivity, a subsidence crater may be the most desirable method of producing the desired surface depression. Also, because more explosive is needed to produce subsidence craters, the method will become more valuable as the cost of nuclear explosives decreases.

Results of the study delineated in the following pages indicate that the prediction of cavity radii can be greatly improved by relating the physical properties of the geologic medium to the material constants (C values) obtained from contained nuclear explosions. The dimensions of subsidence craters can also be more accurately determined from these

physical properties in conjunction with a "bulking" theory. It was also found that measured cavity radii are not necessarily representative of true cavity geometry. An approximate analysis for the determination of collapse times shows that collapse time is greatly dependent on the strength properties of the geologic material, and therefore is subject to large variations in nonuniform material.

From the resulting crater dimensions (volume, depth, and radius) and collapse time, it is possible to calculate the yield for a given depth of burial (DOB) with a fair degree of reliability. This method may prove to be an inexpensive technique for evaluating yields of contained nuclear explosions.

CHAPTER II

Present Status of Work in Area

Since a subsidence crater formed at the surface is dependent on the underground cavity produced by a nuclear explosion, it is necessary to first study the yield/cavity relation. The formation of such cavities has been discussed in numerous reports.[1,3,16,17,19,20,21]

If one considers the various relations that have been used for predicting cavity radii, a general expression may be written in the form

$$R = C \frac{W^{\alpha}}{(\rho\ DOB)^{\beta}}, \tag{1}$$

where

R = cavity radius

C = a constant depending on the geologic material

W = yield

ρ = mass density of overburden

DOB = depth of burial

α, β = constant exponents.

Boardman, Rabb, and McArthur[3] propose that the constants α and β are 1/3 and 1/4, respectively, or

$$R = C \frac{W^{1/3}}{(\rho\ DOB)^{1/4}}. \tag{2}$$

They also tabulate values of C for the various geologic materials in which tests have been conducted. They conclude that R can be predicted within an error of ±20 percent.

A dimensional analysis by Chabai[7] on the variables in ejection cratering experiments indicates that linear dimensions should scale as $W^{1/3}$, provided that gravity is not important. However, it has been found that $\alpha = 0.3$ is more applicable to the data for ejection cratering. Chabai partly explains this by the fact that if gravity is included in the dimensional analysis, the linear dimensions should then scale as the 1/4 power of the energy of yield, provided that the sonic velocities, c, of the mediums are also scaled.

Since the variables for contained shots are similar to those in ejection cratering experiments, one would expect similar relations among the variables. Nondimensional relations among the various dimensions of subsidence craters have been presented by Vortman.[25] His results indicate that a 1/3-power scaling law is more nearly correct for subsidence craters than for ejection craters.

Rogich and Rich[21] performed a statistical analysis of the yield/cavity radius relation for all shots up to December 16, 1965. They concluded that a single empirical equation,

$$R = 54.92\ W^{0.286}, \tag{3}$$

where

R = cavity radius (ft)

W = yield (kt),

could be used to predict the cavity radius in all materials, independent of DOB. Individual shots are at variance with this prediction by as much as 40 percent, while the 95 percent confidence level includes shots that deviate from the equation by about 30 percent. For an engineering application, such as an underground reservoir, such a deviation could amount to an error in volume of approximately a half-million cubic yards for a 1-megaton yield! Therefore, it would be of great value to have an equation that can more accurately predict the cavity radius for a given yield.

In a preliminary report, Berry[2] related the volume of the subsidence crater to the volume of the cavity by using a "bulking" factor that depends on an average height of drop of the geologic material. This method is being modified to make it more general.

CHAPTER III

Experimental Program

The data used in this report were obtained almost exclusively from contained underground nuclear explosions at the Nevada Test Site (NTS).* The test data pertinent to the present study are tabulated in Volume II. The main source of this information was Reference 22, with corrections and additions made as more information became available. Because of the convenient manner in which the information was presented in Reference 22, a similar form has been used in Vol. II. A brief summary of the field measurements is given in the following paragraphs.

3.1 Determination of Yield

Several methods have been used to determine the yield for a given nuclear explosion. These are:

a. Radio-chemistry (Rad. Chem.)

b. Hydrodynamic determinations

c. Seismic techniques.

Further detailed discussion of these methods can be found in References 4 and 15.

Annual reports published by LASL[11-14] state the yield values that are the most satisfactory for their tests. These results have been used in this analysis. The most recent yield values (Flintlock Series) were obtained via verbal communication with Charles I. Browne, Jr., J-DO, LASL.

*Individual tests were made in Carlsbad, New Mexico (Gnome) and Hattiesburg, Mississippi (Salmon).

The LRL yield determinations presented in Reference 22 were verified and/or corrected through communication with A. F. Clark, LRL.

3.2 Determination of Cavity Radius

Radii of cavities are obtained by postshot drilling techniques. Drill holes through the cavity are referenced to preshot elevations. During cavity formation, a certain thickness of highly radioactive "melt" forms the cavity boundary. Upon cooling, the roof of the cavity collapses, so that the radioactive material drops to the bottom of the cavity chamber. Gamma intensity is determined in the drill hole as a function of depth. The first "peak" in the gamma log occurs when the probe passes through the material that has fallen from the ceiling of the cavity. The lowest peak before return to background defines the bottom boundary of the cavity. By use of data obtained from the gamma log, original cavity size can be computed. It has been the practice to use the outer boundary of the radioactive "melt" when reporting cavity radius, which results in a cavity volume somewhat larger than the volume into which the material above may collapse. If the "melt" is of fairly uniform thickness (i.e., melt formed by heat conduction), the percentage error in the cavity volume would be larger for smaller yields (usually at smaller DOB's). This would appear as a smaller bulking factor, which will be discussed further in Chapter IV.

3.3 Determination of Subsidence Crater Values

The volume of the subsidence crater is calculated from post and preshot contour maps of the area. For some craters, the areas of the contours on a scaled map are planimetered, and volumes are computed by means of the Trapezoidal Rule. The volumes of the remainder of the craters are computed from the Trapezoidal Rule, using vertical "slices."

The depth of the crater is defined as the vertical distance between the preshot ground surface directly above the working point (WP) and the lowest point in the crater. (In a few instances, the lowest point in the crater was not directly above the WP.) This value was also obtained from contour maps. If the original ground elevation above the WP was not given, it was found by interpolating between contours on the

preshot contour map. If no preshot contours were available, the value was found by interpolation of contours beyond the crater boundary on the postshot contour map. The errors involved in these interpolations should be less than 1 foot.

Since the radius at the top of the crater is subject to large variations, a standardized procedure was used in recording this dimension. An average radius was computed from eight radii, each two separated by 45 degrees, for each contour interval. This average was plotted against elevations in the crater. The resulting profile was then extrapolated up to the elevation of the original GZ, and the corresponding radius of the crater determined. This results in a radius that one would expect if the original ground elevation were constant.

Collapse times of the craters were found from geophone records. In a few cases, collapse times were recorded even if no subsidence crater was formed, i.e., if there was subsurface collapse only.

CHAPTER IV

Study of Experimental Data

4.1 General

A procedure similar to Chabai's[7] is used to study the variables that affect the dimensions of the cavity and subsidence crater. It is assumed that average physical properties will describe the medium. (This may be questionable, especially when dimensions of the subsidence crater are considered.) The following quantities are assumed to influence the results (mass, length, time system):

Medium Properties

ρ - mass density of undisturbed medium (ML^{-3})

G - an apparent modulus of the medium ($ML^{-1}T^{-2}$).

Independent Variables

e - distance from explosion center (L)

DOB - depth of burial of nuclear explosive (L)

W or E - mass or energy of explosive (M) or (ML^2T^{-2}).

Dependent Variables

R - radius of cavity (L)

a - radius of crater (L)

V_s - volume of crater (L^3)

h - depth of crater (L)

t_c - collapse time of crater (T).

The apparent modulus of the medium G replaces the yield strength, viscosity, and sonic velocity in Chabai's analysis. It is used to include all moduli for which in situ and dynamic physical descriptions are not obtainable. It is not felt that the sonic velocity is an independent property of the medium, since it is related to some modulus of the material and its mass density (i.e., $c = \sqrt{\text{modulus}/\rho}$). This modulus,

G, is related to the amount of pressure needed to cause a permanent deformation.

Because the modulus G and the energy of the explosive E are the only nondependent variables that contain the time dimension, E (rather than W), will be used in the following dimensional analysis. This is permissible since the yield of a nuclear explosive is based upon the energy released by a certain mass of TNT, and this relationship is linear between W and E.

After performing a dimensional analysis for each of the dependent variables, there results:

$$\frac{R}{DOB} = f_1\left(\frac{E^{1/3}}{G^{1/3}\ DOB}, \frac{E^{1/3}}{G^{1/3}\ e}\right), \tag{4a}$$

$$\frac{a}{DOB} = f_2, \tag{4b}$$

$$\frac{h}{DOB} = f_3, \tag{4c}$$

$$\frac{V_s}{DOB^3} = f_4, \tag{4d}$$

$$t_c\left(\frac{E}{\rho\ DOB^5}\right)^{1/2} = f_5, \tag{4e}$$

for which the arguments of the functions f_2, f_3, f_4, and f_5 are identical to those of f_1. It remains to determine the relationships among the dimensionless ratios.

4.2 Cavity Radius

The volume of radioactive melt produced during the initial stages of cavity growth is only a small fraction of final cavity volume. It is also known that cavity expansion in the hydrodynamic regime is not a strong function of properties of the material involved. However, it seems reasonable that cavity growth in the "plastic" state would be strongly influenced by the physical properties of the material. The modulus, G, has been included in the present analysis as representing these properties.

Because information is not available to determine the modulus, G, for each shot, it is only possible to compare data from tests for which G would have similar values. It seems reasonable that geologic materials having similar physical properties might be found immediately above or below a boundary separating two strata. Fortunately, the depth to the alluvium-tuff interface has been recorded for most shots, and this measurement will be utilized in the following analysis.

To find the relations among the dimensionless parameters in Eq. (4a), two of the ratios will be compared (R/DOB, $E^{1/3}/G^{1/3}$ DOB) while the remaining argument ($E^{1/3}/G^{1/3}e$) is kept constant. (Although the relationship between e and $E^{1/3}$ is not known at this point in the analysis, it will be found that $R \propto E^{1/3}$, and therefore $e \propto E^{1/3}$ when the cavity radius is being considered.)

Direct measurement of physical characteristics of media at shot depth were not obtained; hence G could not be determined directly. On the basis of conversations with USGS personnel, it was decided that tuff immediately below, or alluvium directly above, the alluvium-tuff interface would be similar from one location to another. Thus it was assumed there would be one constant for G for shots just above, and another constant for shots just below, the interface. Data available for analysis were limited after elimination of shots which vented, were fired in a "room," or which had cavities intersecting the water table.

Shots selected for analysis were further limited as follows. Shots below the interface were restricted to those with a center of explosion in tuff within 150 feet of the interface. Three shots in tuff were chosen where cavity radius penetrated a short distance into alluvium,

on the assumption that the downward radius of the cavity (the only radius measured) was not affected. Shots in alluvium were limited to those with a cavity bottom within 150 feet of the interface. The distance from cavity bottom to the interface ranged from 0.04 to 1.14 cavity radii. It might be expected that shock reflection off the tuff would limit downward cavity growth. Yet for two shots at essentially the same burial depth, that which was 0.04 cavity radius from the interface had a larger scaled cavity radius than one with a cavity separated from the interface by 1.14 cavity radii. This suggests that other factors are of greater influence on cavity radius than the presence of the interface.

The relationships between cavity radius R, yield W*, and depth of burial (DOB) for shots in the vicinity of the alluvium-tuff interface are shown in Figure 1. G is not included in the abscissa because it is assumed to be constant and its value is unknown. Although DOB's in alluvium varied from 633 to 1663 feet, the linear nature of the plot passing through the origin in Figure 1a suggests that DOB does not affect the results.** The same point is illustrated by the plot in Figure 1b. The DOB values in tuff varied from 470 to 867 feet, but once again, the relation is linear and no depth effects can be seen. This independence of depth was also found by Rogich and Rich.[21]

As an independent calculation to determine scaling for shots at this geologic boundary, the cavity radius-yield relations are plotted in Figure 2. The method of least squares was used to determine the best fit to the data. The exponent was 0.325 ± 0.015 for shots in alluvium and 0.329 ± 0.026 for tuff. Therefore, it was concluded that cube-root scaling applies for a <u>given</u> material.

*Because of the linear relation between W and E, and because W is readily available for all shots, W will be used hereafter as a measure of yield.

**Small depth effects are difficult to isolate because, in general, the larger yields occurred at greater depths.

[redacted]

UNCLASSIFIED

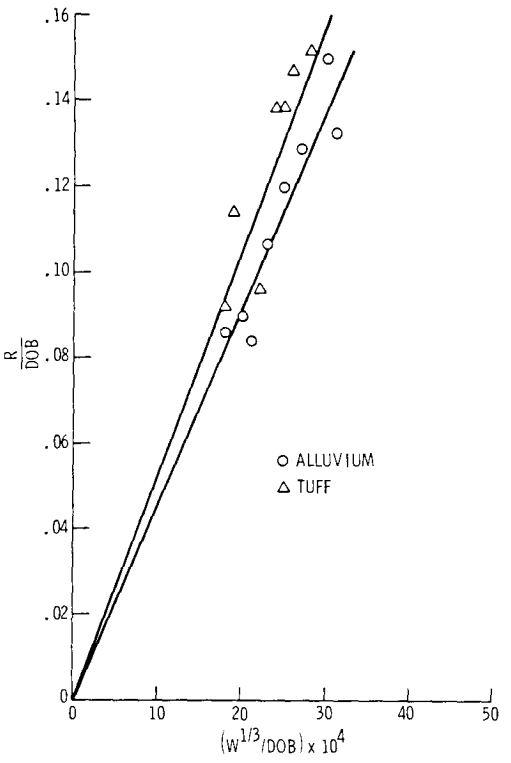

(a)

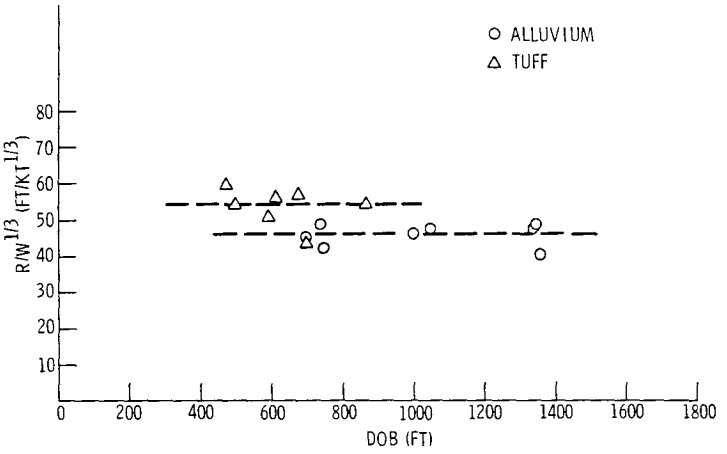

(b)

Figure 1. Relationships among R, W, and DOB at alluvium-tuff interface

UNCLASSIFIED

[redacted]

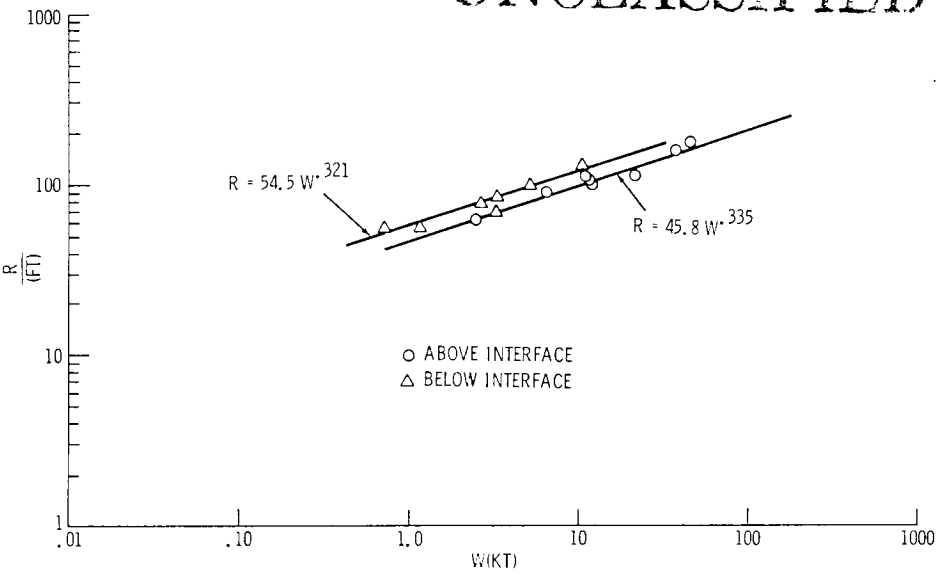

Figure 2. Cavity radius vs yield at alluvium-tuff interface

Note that the cavity radii in the tuff in Figure 2 are approximately 20 percent larger than in the alluvium; i.e., the modulus, G, is smaller for tuff than for alluvium. It is possible that the shallower shot depths in tuff, and thus the influence of the free boundary, might account for this variance; but it is very unlikely that it would account for such a large variation, expecially since the same difference exists between individual shots in alluvium and tuff at the same depths. More likely, these results indicate the effect of the physical properties of the medium. (This effect is also shown in Figure 1.)

Thus, the size of the cavity may be predicted from the equation

$$R = CW^{1/3}, \tag{5}$$

where

R = cavity radius (ft)

W = yield of nuclear explosive (kt)

C = constant dependent on the geologic medium ($ft/kt^{1/3}$).

From the discussion on dimensionality, it can also be seen that C is inversely proportional to $G^{1/3}$. Equation (5) predicts the measured cavity radius. (The possibility of the cavity not being spherical is discussed in later sections.)

Assuming the validity of Eq. (5), C values for the various materials may be calculated for all shots at NTS having yields and radii given. These values are shown in Table I.

TABLE I

Material Constants for Various Media

Medium	C(ft/kt$^{1/3}$)
Alluvium	30 to 70*
Tuff	30 to 70
Basalt (1 shot)	~48
Granite (2 shots)	~37
Dolomite (1 shot)	~30
Salt (2 shots)	~32

*U3ab (Ermine) had a C value of 85, but the measurements of the 12-foot cavity radius might be in error

The constant, C, varies widely within the materials described as alluvium and tuff (C ≈ 30 to 70). Three of the shots in alluvium at large burial depths (Agouti, Chinchilla I, and Paca) had C values between 63 and 66. In each case, geologic investigations indicated a "weak" core sample and/or inconsistencies in the sonic log at the burial depth.[5,6,9,26,27] Also, the shots in welded tuff and in materials described as zeolitized had smaller C values than soft-bedded or friable tuff. Thus, the existence of a correlation between the physical properties of the material and the value of C should not be excluded. Possibly a relation may be found between C and the stress-strain relations in a standard triaxial test with a confining pressure proportional to the overburden pressure. (This might even include the overburden surface effects in the determination of C.) A predetermined value of C obtained from the physical and mechanical properties of the geologic material would possibly eliminate much of the scatter in the data discussed in Chapter II.

It is interesting to note that the lower limit of the C values in alluvium and tuff is similar to that in basalt, granite, dolomite, and salt. This would indicate that certain types of alluvium and tuff provide as much resistance to cavity growth as do these other media.

Not enough data were available to determine the effect of a water-saturated soil on the cavity radius, nor was it possible to detect any effect related to distance from a fault.

Substituting the relation $C \propto 1/G^{1/3}$ and $W \propto E$, Eqs. (4b) to (4e) may be rewritten,

$$a/DOB = f_2'\left(CW^{1/3}/DOB,\ CW^{1/3}/e\right) \tag{4b'}$$

$$h/DOB = f_3'\left(CW^{1/3}/DOB,\ CW^{1/3}/e\right) \tag{4c'}$$

$$V_s/DOB^3 = f_4'\left(CW^{1/3}/DOB,\ CW^{1/3}/e\right) \tag{4d'}$$

$$t_c\left(W/\rho\, DOB^5\right)^{1/2} = f_5'\left(CW^{1/3}/DOB,\ CW^{1/3}/e\right) \tag{4e'}$$

or from Eq. (5)

$$a/DOB = f_2''\left(R/DOB,\ CW^{1/3}/e\right) \tag{4b''}$$

$$h/DOB = f_3''\left(R/DOB,\ CW^{1/3}/e\right) \tag{4c''}$$

$$V_s/DOB^3 = f_4''\left(R/DOB,\ CW^{1/3}/e\right) \tag{4d''}$$

$$t_c\left(W/\rho\, DOB^5\right)^{1/2} = f_5''\left(R/DOB,\ CW^{1/3}/e\right). \tag{4e''}$$

Thus, when finding the relations between a/DOB vs R/DOB, h/DOB vs R/DOB, ..., it is necessary to keep the argument $(CW^{1/3}/e)$ constant.

4.3 Subsidence Craters

Contrary to the results found for cavity radii, one might expect the size of the subsidence crater to be dependent upon DOB. If a device of a given yield were detonated at a very great depth (large R/DOB), no subsidence crater would result. One may predict this by using a theory of bulking in the material.

It is assumed that the contained nuclear explosion disturbs the surrounding medium (particularly above the shot) adequately to reduce its cohesive and frictional strength so that it is essentially free to fall into the cavity, when the cavity pressure is reduced to some value less than that of the overburden. If disturbance of the soil mass does not propagate to the surface, it is possible that a void may be created at the top of the chimney, supported by "arching" action of the soil. (It is assumed that this arching action is temporary and can be removed by vibration, etc.)

The data from the subsidence crater dimensions indicate that for depths of burial deeper than some critical value of DOB/R, no subsidence occurs. The data also indicate a high variability in crater volume for a given DOB/R. In the following analysis this variability will be ignored and an average bulking factor calculated. If arching is a significant factor in the indicated variability, then the average bulking factor calculated would be that due to normal bulking plus that contributed by arching. The significance of this high variability will not be pursued further in this report but should be considered in studies of the usefulness of subsidence craters for practical excavation projects.

In general, the material which falls into the cavity will increase in volume (bulk) to a value

$$B \times (\text{undisturbed volume}),^{*} \qquad (6)$$

* "Undisturbed" refers to the soil mass after formation of the cavity, but before collapse.

where B is the bulking factor. If the failure surface is approximated by the frustum of a cone (Figure 3a), the height d_c to which the chimney will propagate will depend on B:

$$\left\{\frac{\pi d_c}{3}\left[R^2 + \left(R + d_c \tan\theta\right)^2 + R\left(R + d_c \tan\theta\right)\right] - \frac{2}{3}\pi R^3\right\}B = \frac{\pi d_c}{3}\left[R^2 + \left(R + d_c \tan\theta\right)^2 + R\left(R + d_c \tan\theta\right)\right] + \frac{2}{3}\pi R^3 \tag{7}$$

or

$$B = \frac{d_c\left[R^2 + \left(R + d_c \tan\theta\right)^2 + R\left(R + d_c \tan\theta\right)\right] + 2R^3}{d_c\left[R^2 + \left(R + d_c \tan\theta\right)^2 + R\left(R + d_c \tan\theta\right)\right] - 2R^3} . \tag{8}$$

Since it is very difficult to determine chimney height for shots which do not subside at the surface, the bulking factor B may be found from shots in which the chimney just reaches the surface, i.e., $d_c = (DOB)_c$. Therefore,

$$B = \frac{(DOB)_c\left[R^2 + \left(R + DOB_c \tan\theta\right)^2 + R\left(R + DOB_c \tan\theta\right)\right] + 2R^3}{(DOB)_c\left[R^2 + \left(R + DOB_c \tan\theta\right)^2 + R\left(R + DOB_c \tan\theta\right)\right] - 2R^3} \tag{9}$$

or

$$B = \frac{\left(\frac{DOB}{R}\right)_c\left[1 + \left\{1 + \left(\frac{DOB}{R}\right)_c \tan\theta\right\}^2 + \left\{1 + \left(\frac{DOB}{R}\right)_c \tan\theta\right\}\right] + 2}{\left(\frac{DOB}{R}\right)_c\left[1 + \left\{1 + \left(\frac{DOB}{R}\right)_c \tan\theta\right\}^2 + \left\{1 + \left(\frac{DOB}{R}\right)_c \tan\theta\right\}\right] - 2} \tag{10}$$

where $(DOB/R)_c$ is the smallest value of (DOB/R) for which no subsidence occurs (i.e., "critical" DOB/R).

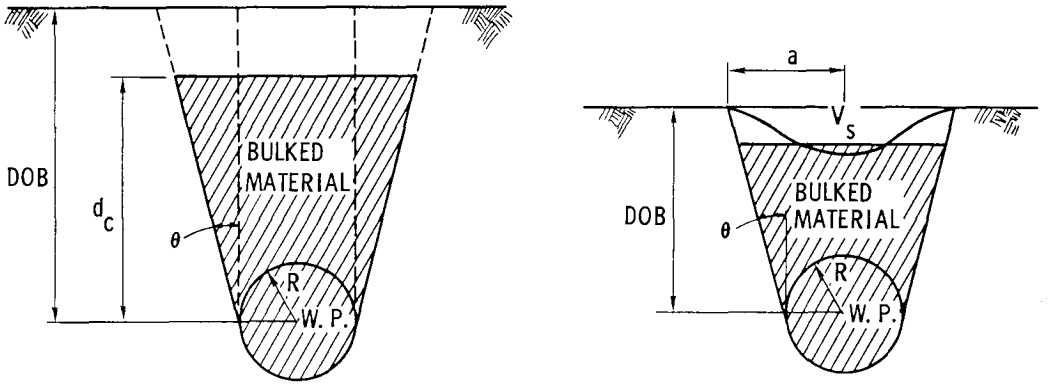

a. NO SUBSIDENCE b. SUBSIDENCE

Figure 3. Chimneys formed by underground explosions

In the following analysis, it will be assumed that the bulking factor B is constant. This assumption may appear questionable, since the degree of compaction should depend somewhat upon the height of fall of the material. Doubtless there are variations in the degree of compaction throughout the soil column above the cavity, requiring the bulking factor to be an average for the material. On the basis of the behavior of a dry, granular soil, the maximum density is obtained with a free fall of just a few feet. Therefore, it seems reasonable to assume B as a constant for a particular area, especially since variations in the scaled burial depth ($DOB/W^{1/3}$) are not extreme.

Investigations were made for four different areas at NTS, from which enough experimental data were available to give a statistical average. These areas included Areas 2 (alluvium), 3 (alluvium), and 9 (alluvium and tuff below alluvium).

Plotted in Figures 4 through 7 are subsidence crater volumes versus DOB/R. From the critical DOB/R (smallest DOB/R for which no subsidence crater forms), the bulking factor for each area can be found using Eq. (10). These values are tabulated in Table II. The average of the measured values of tan θ (Table IV) (computed from measured-cavity and subsidence-crater radii, assuming geometry of Figure 3b) was used in computing the bulking factors for each area.

TABLE II

Bulking Factors for Various NTS Areas

Area	Material	B Eq. (10)
2	Alluvium	1.07
3	Alluvium	1.01
9	Alluvium	1.04
9	Tuff below alluvium	1.04

The possibility that measured cavity radius R is not a true indicator of cavity size is discussed in Paragraph 4.3.1. An uncertainty in R, or in any other effect on the value of the bulking factor, may not appear large, but it is to be remembered that a small change in B can result in a very significant change in the resulting crater.

4.3.1 Crater Volumes

If $(DOB/R) < (DOB/R)_c$, subsidence craters will form. The volume of these craters may also be determined from B. Referring to Figure 3b,

$$\left\{\frac{\pi \cdot DOB}{3}\left[R^2 + (R + DOB \tan\theta)^2 + R(R + DOB \tan\theta)\right] - \frac{2}{3}\pi R^3\right\} B - V_s =$$

$$\frac{\pi \cdot DOB}{3}\left[R^2 + (R + DOB \tan\theta)^2 + R(R + DOB \tan\theta)\right] + \frac{2}{3}\pi R^3 \quad (11)$$

or

$$V_s = \frac{2\pi R^3 (B + 1)}{3} - (B - 1)\frac{\pi}{3} \cdot DOB\left[R^2 + (R + DOB \tan\theta)^2 + R(R + DOB \tan\theta)\right], \quad (12)$$

where V_s = volume of the subsidence crater.

The volumes of the subsidence craters V_s may be compared to the volumes of the assumed spherical cavity V_c:

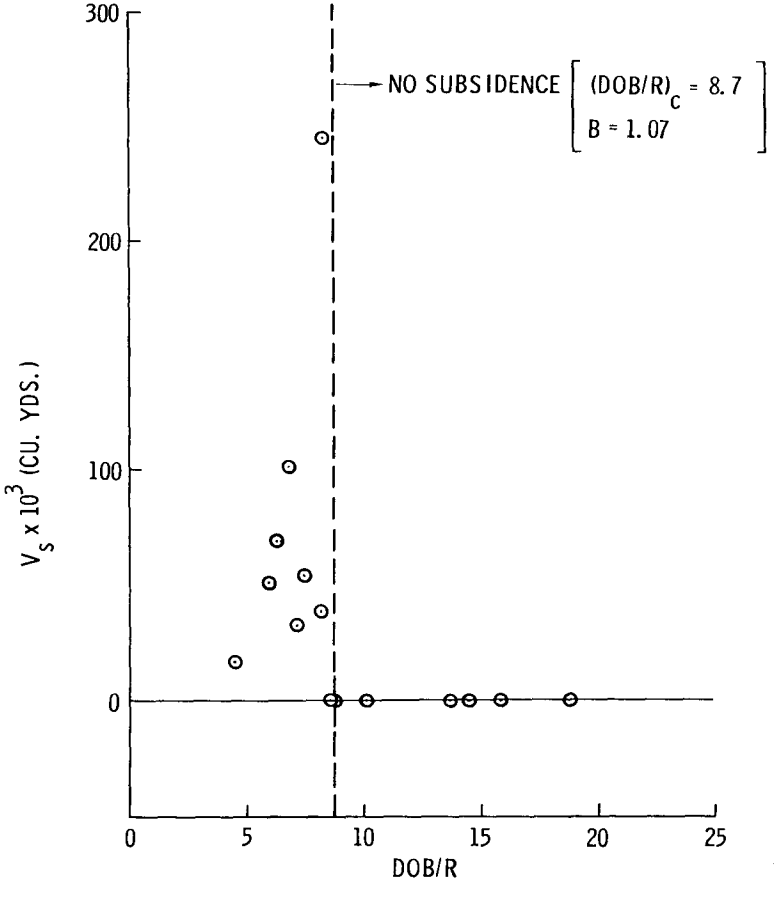

Figure 4. Subsidence crater volumes vs DOB/R (Area 2 - alluvium)

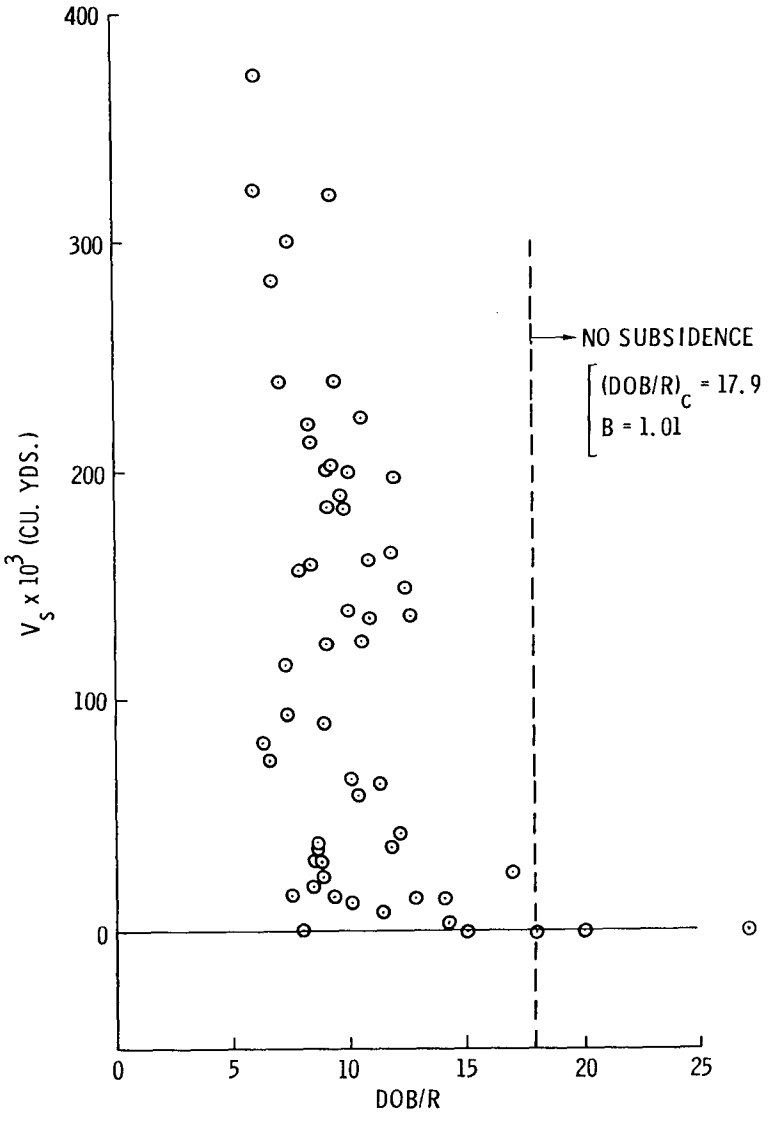

Figure 5. Subsidence crater volumes vs DOB/R (Area 3 - alluvium)

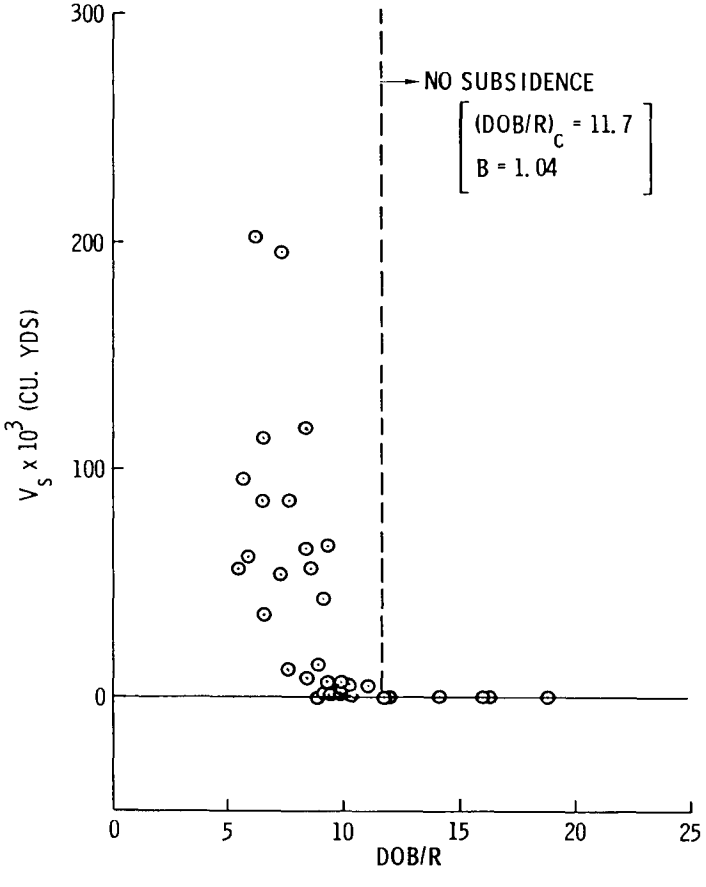

Figure 6. Subsidence crater volumes vs DOB/R (Area 9 - alluvium)

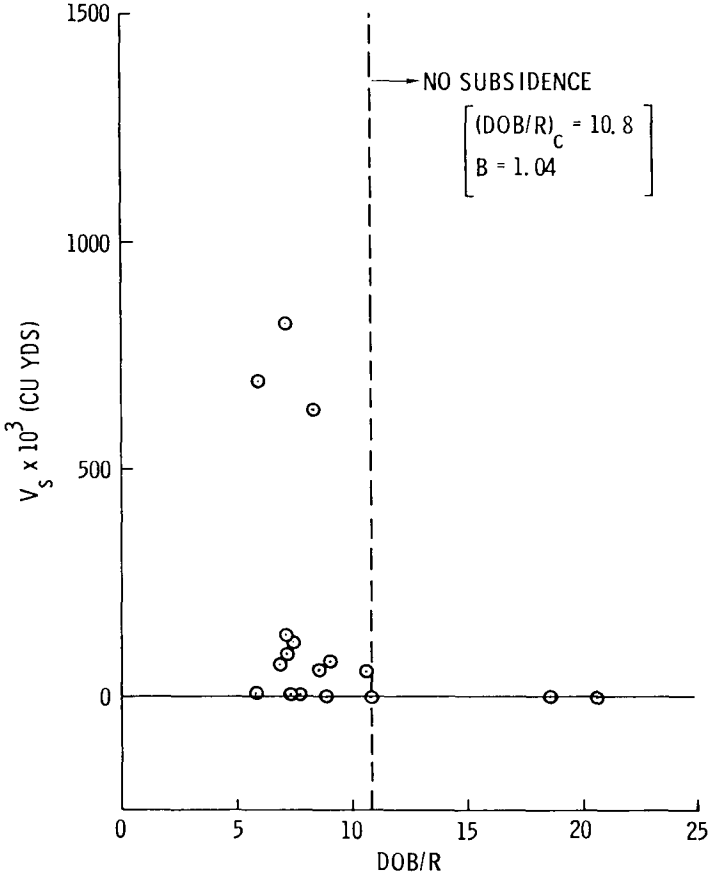

Figure 7. Subsidence crater volumes vs DOB/R (Area 9 - tuff below alluvium)

$$\frac{V_s}{V_c} = \frac{V_s}{\frac{4}{3}\pi R^3} = \frac{B+1}{2} - \frac{3(B-1)}{4}\left(\frac{DOB}{R}\right) - \frac{3(B-1)\tan\theta}{4}\left(\frac{DOB}{R}\right)^2 - \frac{(B-1)\tan^2\theta}{4}\left(\frac{DOB}{R}\right)^3. \quad (13)$$

It is readily seen that if no bulking occurs (B = 1), then $V_s/V_c = 1$, or the volume of the crater equals that of the cavity. Only when the cavity radius is underestimated, or B < 1 (increase in density), will the ratio exceed a value of one.

Equation (13) is valid for $L < (DOB/R) < (DOB/R)_c$. (DOB/R) is bounded by a lower limit L, since a very small DOB/R will produce an ejection crater. The Sedan ejection crater (Area 10) is plotted in Figures 8a, 9a, 10a, and 11a.

Various other dimensionless ratios can be formed from the variables besides those given by Eq. (4). Preliminary investigations included a study of the relations between the arguments given in Table III. The relations are listed in decreasing degree of scatter (i.e., based on the "coefficient of determination"), with a relative scatter value given. As discussed previously, it is necessary to keep $(CW^{1/3}/e)$ constant when studying any given relation. However, the scatter in the data was such that no distinction could be made for different values of this argument, and thus all points were included.

TABLE III

Volume Relations for Subsidence Craters

Relation				Relative Scatter*
(1)	$\frac{V_s}{\frac{4}{3}\pi R^3}$	vs	$\frac{DOB}{R}$	3.83
(2)	$\frac{V_s}{W}$	vs	$\frac{DOB}{R}$	1.66
(3)	$\frac{V_s}{W}$	vs	$\frac{DOB}{W^{1/3}}$	1.65
(4)	$\frac{V_s}{DOB^3}$	vs	$\frac{R}{DOB}$	1.28
(5)	$\frac{V_s}{DOB^3}$	vs	$\frac{W^{1/3}}{DOB}$	1.00

*The relative scatter values are averages of all four areas that were considered (Paragraph 4.3), the coefficient of determination of each area being weighted according to the number of experimental points. Relation (5) above is assumed to have a value of 1.00.

The equations corresponding to the relations in Table III are, respectively,

$$(1)\quad \frac{V_s}{V_c} = \frac{B+1}{2} - \frac{3(B-1)}{4}\left(\frac{DOB}{R}\right) - \frac{3(B-1)\tan\theta}{4}\left(\frac{DOB}{R}\right)^2 - \frac{(B-1)\tan^2\theta}{4}\left(\frac{DOB}{R}\right)^3 \qquad (13)$$

$$(2)\qquad \frac{V_s}{W} = \frac{2\pi C^3(B+1)}{3} - \pi C^3(B-1)\left(\frac{DOB}{R}\right) - \pi C^3(B-1)\tan\theta\left(\frac{DOB}{R}\right)^2 - \frac{\pi C^3(B-1)\tan^2\theta}{3}\left(\frac{DOB}{R}\right)^3 \qquad (14)$$

$$(3)\qquad \frac{V_s}{W} = \frac{2\pi C^3(B+1)}{3} - \pi C^2(B-1)\left(\frac{DOB}{W^{1/3}}\right) - \pi C(B-1)\tan\theta\left(\frac{DOB}{W^{1/3}}\right)^2 - \frac{\pi(B-1)\tan^2\theta}{3}\left(\frac{DOB}{W^{1/3}}\right)^3 \qquad (15)$$

$$(4)\qquad \frac{V_s}{DOB^3} = \frac{2\pi}{3}\left(\frac{R}{DOB}\right)^3 - \pi(B-1)\left(\frac{R}{DOB}\right)^2 - \pi(B-1)\tan\theta\left(\frac{R}{DOB}\right) - \frac{\pi(B-1)\tan^2\theta}{3} \qquad (16)$$

$$(5)\qquad \frac{V_s}{DOB^3} = \frac{2\pi C^3}{3}\left(\frac{W^{1/3}}{DOB}\right)^3 - \pi C^2(B-1)\left(\frac{W^{1/3}}{DOB}\right)^2 - \pi C(B-1)\tan\theta\left(\frac{W^{1/3}}{DOB}\right) - \frac{\pi(B-1)\tan^2\theta}{3} \qquad (17)$$

The average C, ($\bar{C}$), and average tan θ were used for each area in the above equations when theoretical values were related to experimental results. These values are given in Table IV.

In Paragraph 4.3.2 it is found that tan θ is actually a function of scaled burial depth ($DOB/W^{1/3}$), although the scatter is quite large. The inclusion of these relations (Eqs. 28 through 31) improves the correlation for Eqs. (13) through (17) at large scaled burial depths, but decreases it at small scaled burial depths. Therefore the average tan θ given in Table IV was used.

TABLE IV

Average Values for C and tan θ for Various NTS Areas

Area	2A*	3A*	9A*	9T*
Average $C(ft/kt^{1/3})$, $\overline{C}$	50.05	55.05	50.02	51.52
Average tan θ	0.108	0.158	0.124	0.144

*A = alluvium
T = tuff below alluvium.

One possibility for the above discrepancy is the scatter in the experimental data in determining tan θ (Figures 12 through 15). Since the computed volumes in Eqs. (13) through (17) are very sensitive to the bulking factor B, and in turn, the bulking factor depends on the tan θ corresponding to the $(DOB/R)_c$ . . ., determination of the correct tan θ becomes essential. Also, variations in the assumed constant value of B become a major factor.

Note (Table III) that as the scatter becomes less, the influence of the cavity radius, R, in the above relations also decreases. The "best fit" relation (V_s/DOB^3) versus $(W^{1/3}/DOB)$, does not even contain R. This would indicate that the measured R is not always a reliable indicator of true cavity geometry.

The relations between the volumes of the subsidence craters and the assumed cavity volumes (Eq. (13)), together with the experimental points for each area, are given in Figures 8a, 9a, 10a, and 11a. Figures 8b, 9b, 10b, and 11b are plots of the experimental points against the theoretical equation (Eq. (17)). As indicated by Table III, the scatter about the theoretical curves is much less in Figures 8b, 9b, 10b, and 11b than in Figures 8a, 9a, 10a, and 11a. In fact in the latter cases, it is not clear from direct comparisons of the data and the curve, that the curve is even of the proper form. However, the scatter in Area 9 is much less than in Area 3 when the cavity radius relations are used (Figures 9a and 10a).

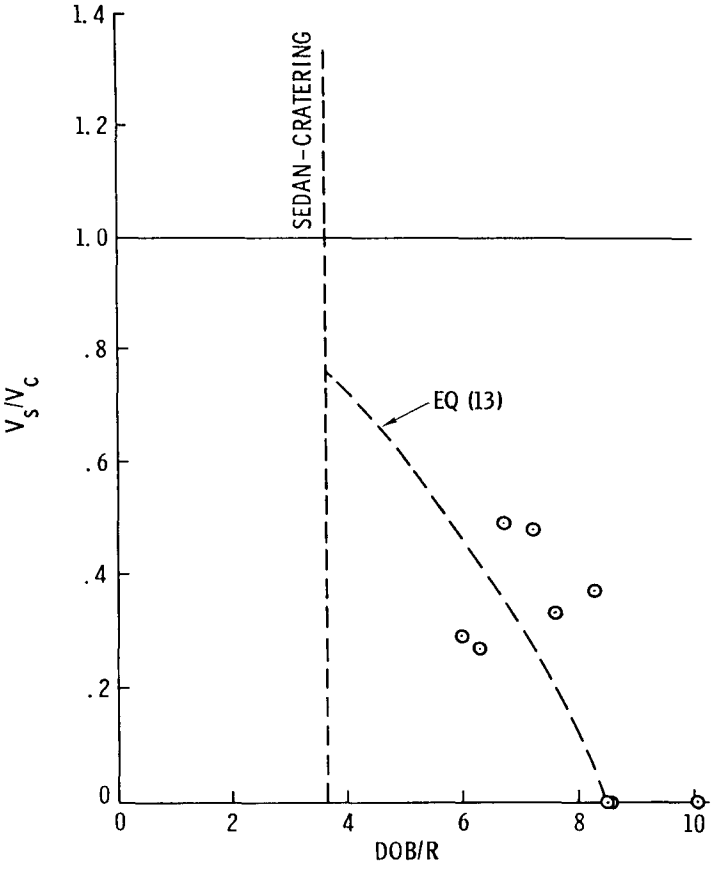

a. V_S/V_C vs DOB/R

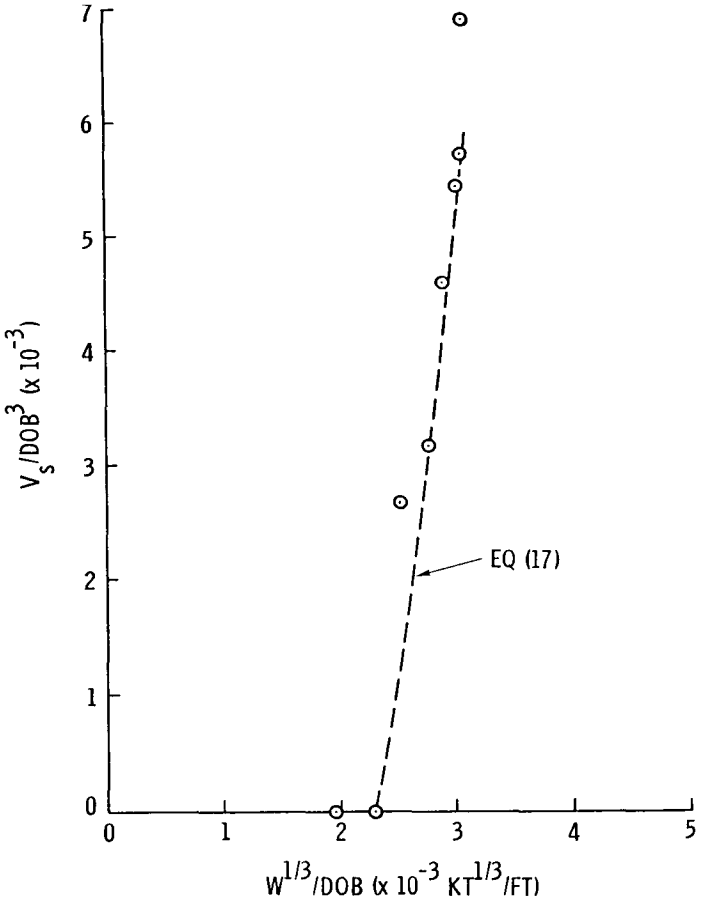

b. V_S/DOB^3 vs $W^{1/3}/DOB$

Figure 8. Area 2 - alluvium

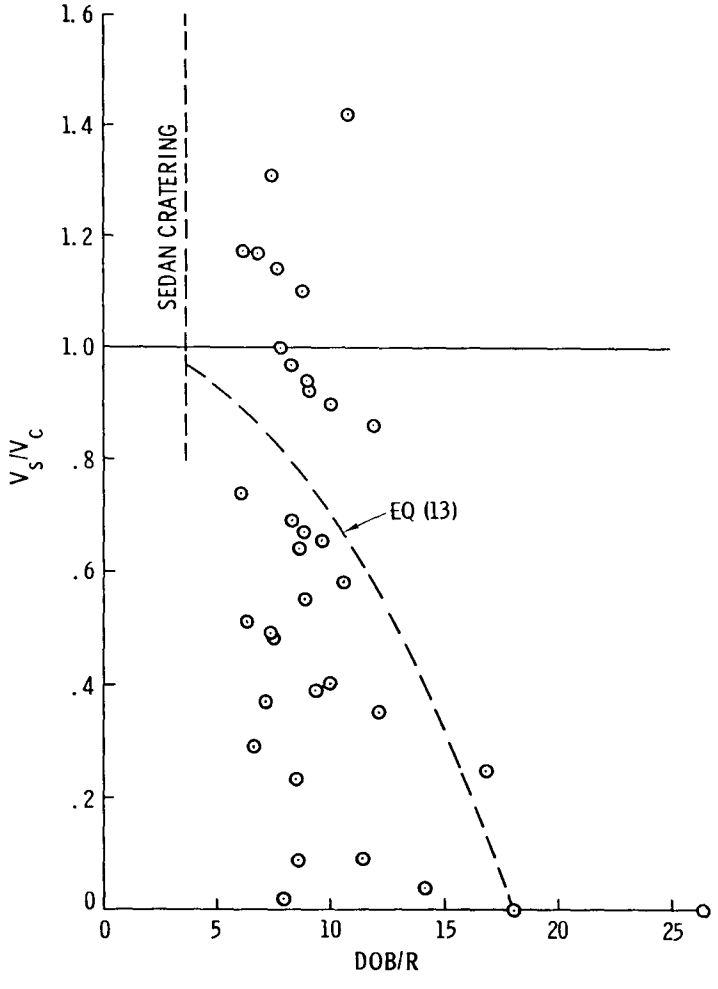

a. V_S/V_C vs DOB/R

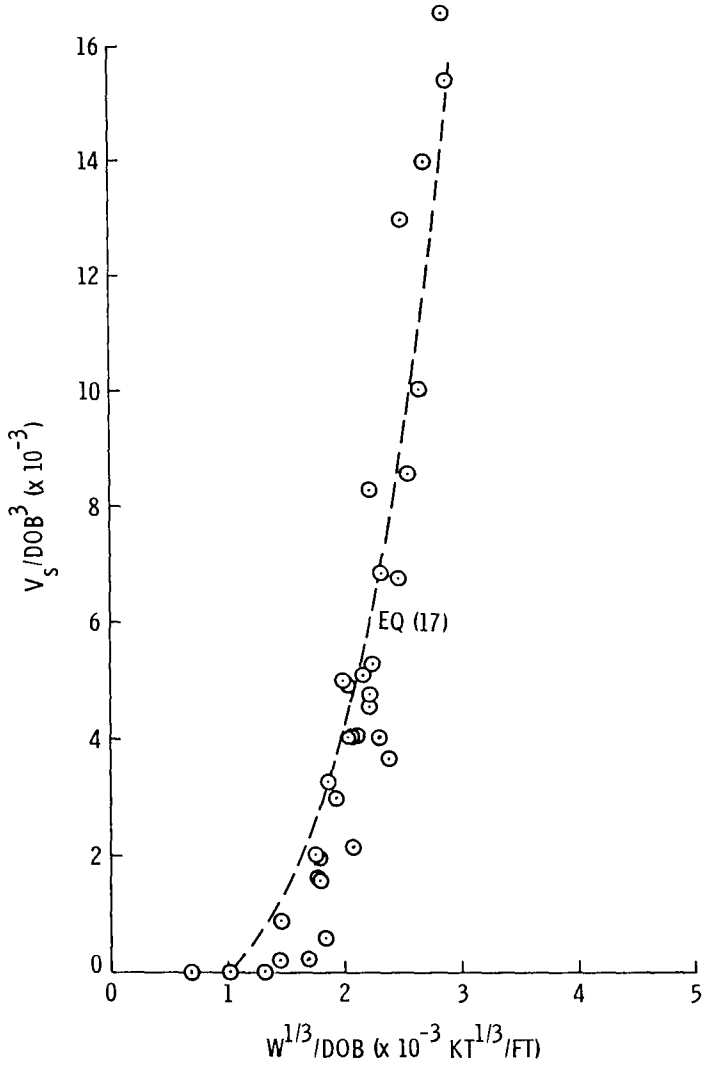

b. V_S/DOB^3 vs $W^{1/3}/DOB$

Figure 9. Area 3 - alluvium

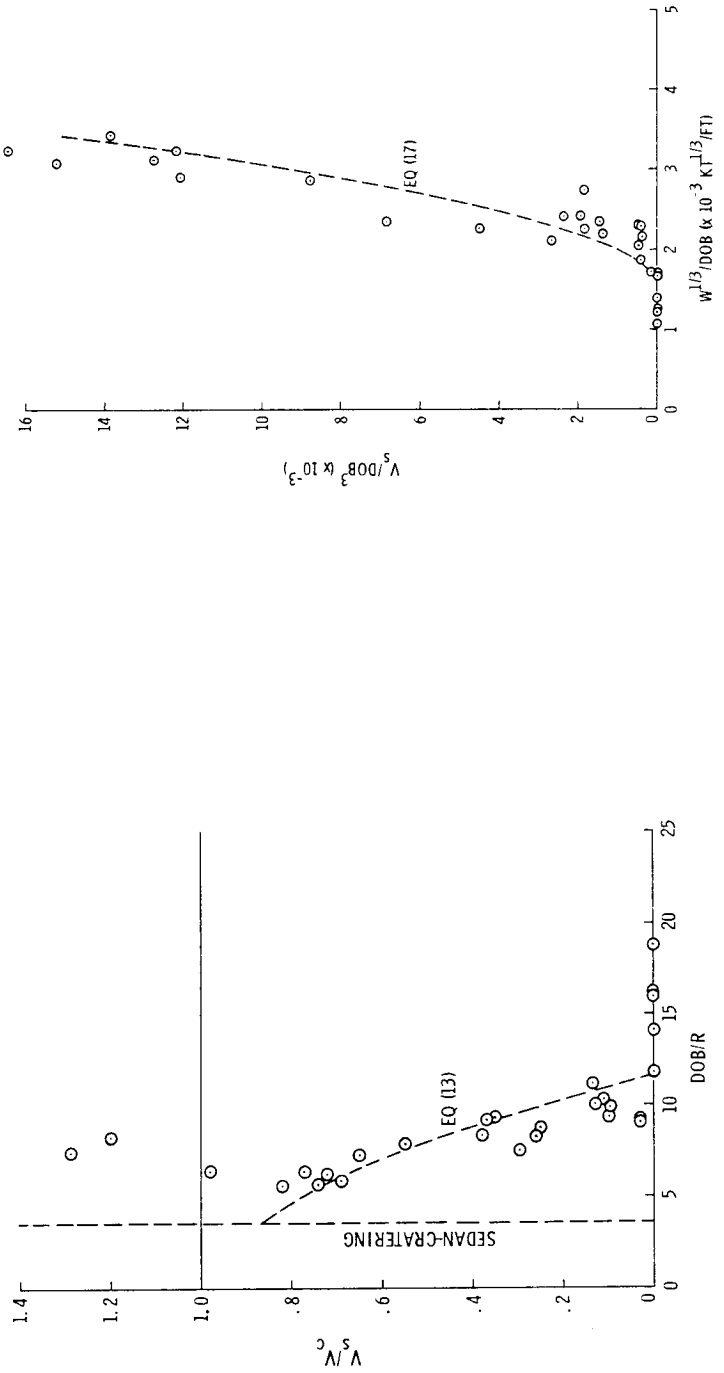

b. V_S/DOB^3 vs $W^{1/3}/DOB$

a. V_S/V_C vs DOB/R

Figure 10. Area 9 - alluvium

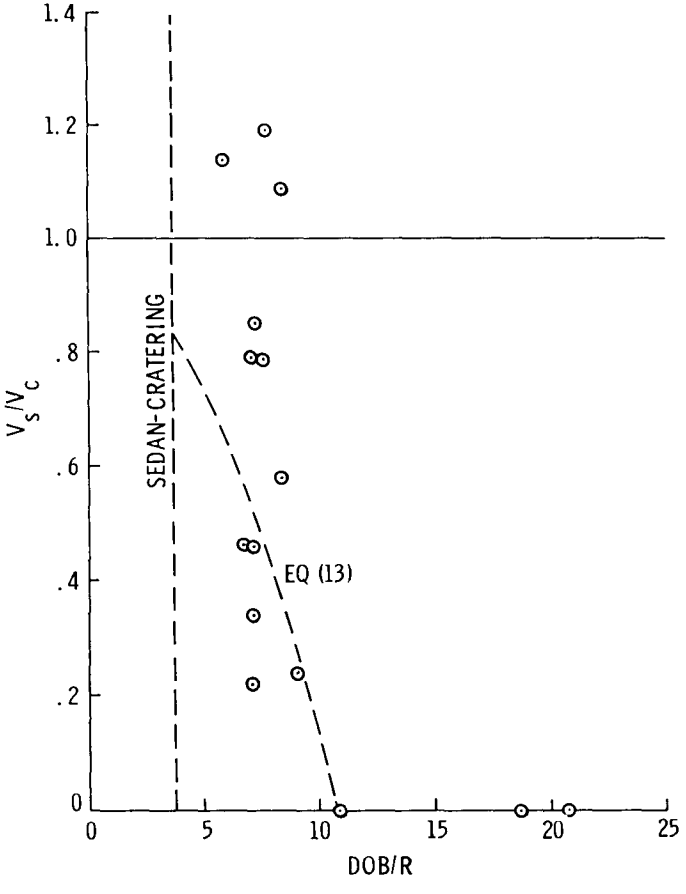

a. V_s/V_c vs DOB/R

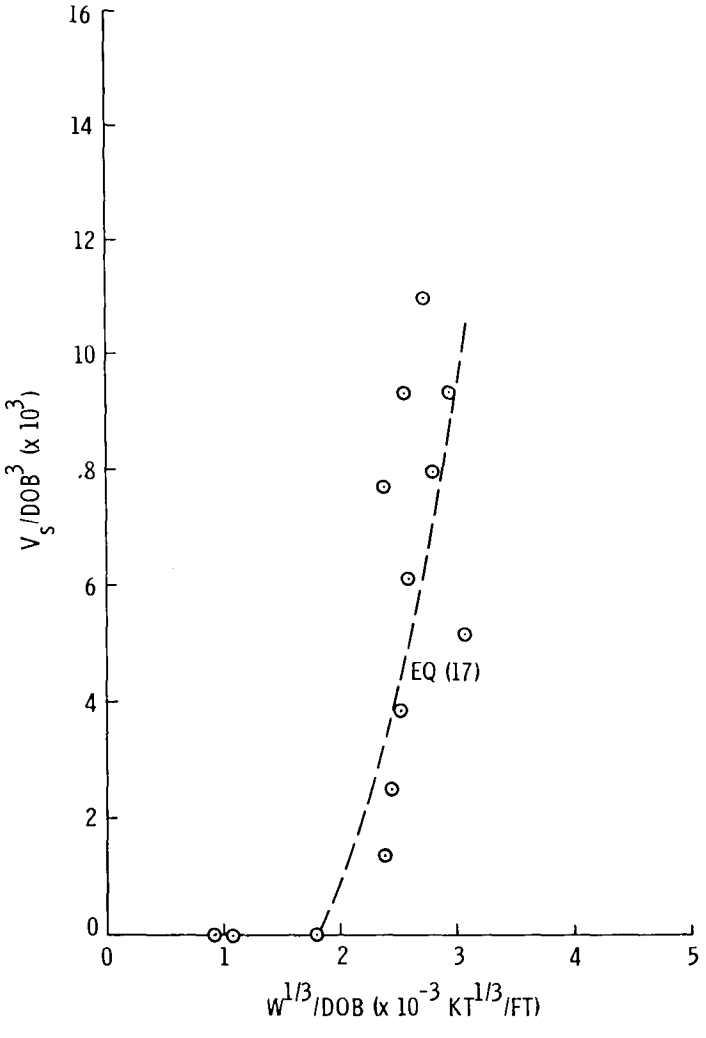

b. V_s/DOB^3 vs $W^{1/3}/DOB$

Figure 11. Area 9 - tuff below alluvium

Note in Figures 9a, 10a, and 11a that the volumes of the subsidence craters occasionally exceed those of assumed spherical cavities. Since it is unlikely that the bulking factor B is less than unity, and because the measured R is probably overestimated (Paragraph 3.2), the results indicate that the cavity is probably not spherical, but may be asymmetric, with the larger dimension toward the free surface. If the cavity is asymmetric in the vertical direction, the measured R would give a volume ($4/3\pi R^3$) which is too small. This possibility appears reasonable when Cherry's work[8] is considered. This, in conjunction with variations in the physical properties of the medium, may account for the large scatter when measured cavity radius R is included in the relations (Eqs. (13) through (17)). Even when R is not included in the relations, the remaining scatter is probably due to variations in physical properties. However, the results do indicate that the yield W is a better indicator of cavity size than measured cavity radius.

Although the bulking theory gives a reasonable physical meaning to the relations, for the reasons listed above, inclusion of the measured R increases the scatter and thus reduces the reliability of the equation (Eq. (13)). If a correlation among the physical characteristics of the medium (including DOB), cavity geometry, and yield can be made, this relation may prove the superior one. However, in the absence of these correlations, the most reliable results are given by Eq. (17).

Since shots in alluvium in Areas 3 and 9 contained the most data points, it is of interest to compare the volumes of the subsidence craters in these areas. It can be seen from Figures 9b and 10b that the volumes of the subsidence craters in Area 3 are more than twice those of the craters in Area 9, for the same scaled DOB. This is due to the smaller bulking factor in Area 3 (Table II).

One would conclude from the preceding discussion that measured cavity radius R often is not a true indicator of cavity geometry and that the cavity is probably not spherical.

4.3.2 Crater Radius

In Figure 3b, it can be seen that the crater radius a for the assumed failure surface is given approximately by

$$a = R + DOB \tan \theta, \tag{18}$$

or in various dimensionless forms:

$$\frac{a}{R} = 1 + \left(\frac{DOB}{R}\right) \tan \theta, \tag{19}$$

or

$$\frac{a}{CW^{1/3}} = 1 + \left(\frac{DOB}{R}\right) \tan \theta, \tag{20}$$

or

$$\frac{a}{CW^{1/3}} = 1 + \left(\frac{DOB}{CW^{1/3}}\right) \tan \theta, \tag{21}$$

or

$$\frac{a}{DOB} = \frac{R}{DOB} + \tan \theta, \tag{22}$$

or

$$\frac{a}{DOB} = \frac{CW^{1/3}}{DOB} + \tan \theta. \tag{23}$$

On the basis of the discussion in the preceding section regarding the accuracy of using the measured cavity radius, Eq. (23) should provide the best relation. Plotted in Figures 12 through 15 is (a/DOB) vs ($W^{1/3}$/DOB) for each area. Because of the large amount of scatter in the data, curves higher than the first order are probably not justified. Therefore, linear least-square fits were made for the data. These relations are given in Table V.

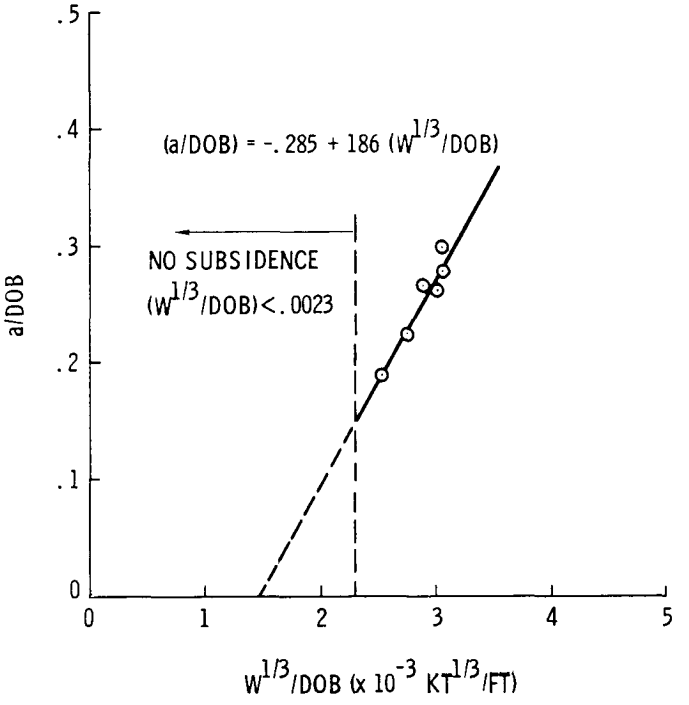

Figure 12. a/DOB vs $W^{1/3}$/DOB (Area 2 - alluvium)

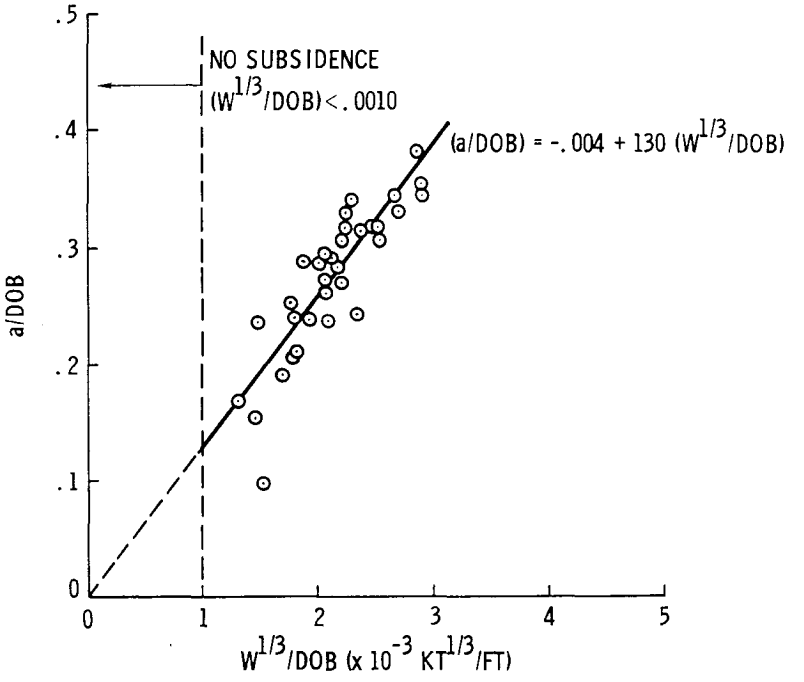

Figure 13. a/DOB vs $W^{1/3}$/DOB (Area 3 - alluvium)

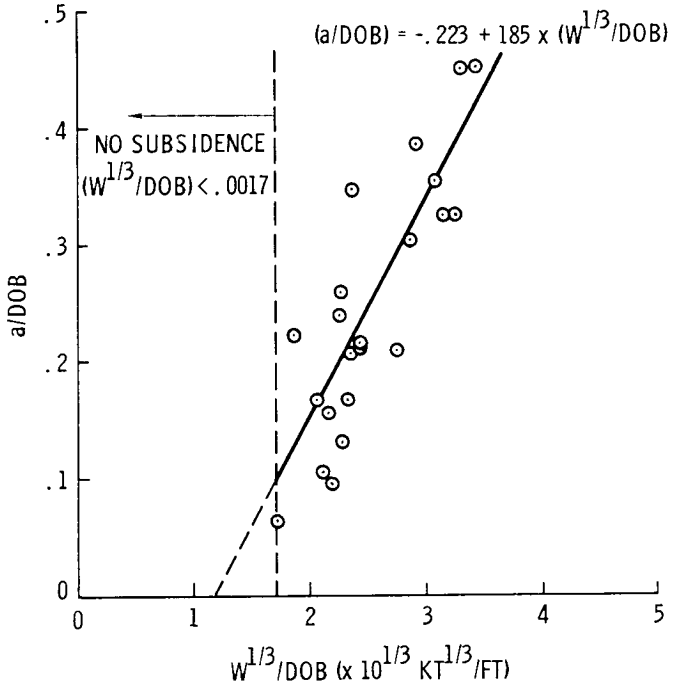

Figure 14. a/DOB vs $W^{1/3}$/DOB (Area 9 - alluvium)

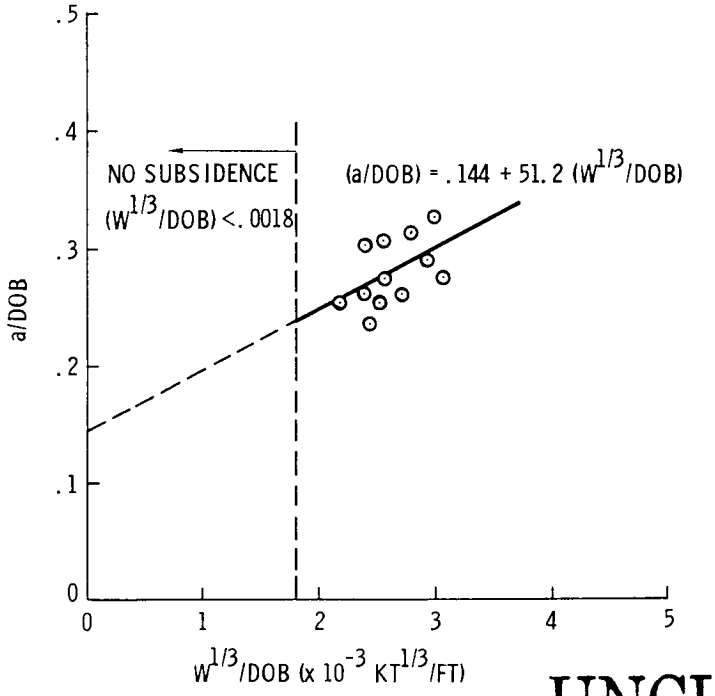

UNCLASSIFIED

Figure 15. a/DOB vs $W^{1/3}$/DOB (Area 9 - tuff below alluvium)

TABLE V

Relations for Determining Crater Radii

Area*	Relation	Eq. No.
2A	$a/DOB = -0.285 + 186\ (W^{1/3}/DOB)$	(24)
3A	$= -0.004 + 130\ (W^{1/3}/DOB)$	(25)
9A	$= -0.223 + 185\ (W^{1/3}/DOB)$	(26)
9T	$= +0.144 + 51.2\ (W^{1/3}/DOB)$	(27)

*A = alluvium
T = tuff.

Assuming Eq. (23) to be valid, tan θ can be found. These relations are given in Table VI.

TABLE VI

Expressions for tan θ in Various NTS Areas

Area*	Relation	Eq. No.
2A	$\tan\theta = -0.285 + 131\ (W^{1/3}/DOB)$	(28)
3A	$= -0.004 + 75\ (W^{1/3}/DOB)$	(29)
9A	$= -0.223 + 135\ (W^{1/3}/DOB)$	(30)
9T	$\cong +0.144$	(31)

*A = alluvium
T = tuff.

Thus it can be seen that the failure surface depends upon the scaled DOB.

4.3.3 Crater Depth

Crater depth h may be determined from crater volume if the geometric shape of the crater is known. In general, from Figure 3b,

$$\frac{1}{m}\pi a^2 h = V_s, \tag{32}$$

or

$$h = \frac{mV_s}{\pi a^2}, \tag{33}$$

where m is a constant depending upon the crater profile. If the subsidence crater is cylindrical, $m = 1$; if parabolic, $m = 2$; and if conical, $m = 3$.

The volumes V_s in the relations (Eqs. (13) through (17)) may be substituted into Eq. (33), resulting in the following dimensionless relations:

$$\frac{h}{R} = m\left\{\left[\frac{2(B+1)}{3} - \frac{(B-1)}{3}\frac{DOB}{R}\right]\left[\frac{1}{\left(1 + \frac{DOB}{R}\tan\theta\right)^2}\right] - \frac{(B-1)}{3}\cdot\frac{DOB}{R}\left[\frac{1}{1 + \frac{DOB}{R}\tan\theta}\right] - \frac{(B-1)}{3}\cdot\frac{DOB}{R}\right\} \tag{34}$$

$$\frac{h}{CW^{1/3}} = m\left\{\left[\frac{2(B+1)}{3} - \frac{(B-1)}{3}\frac{DOB}{R}\right]\left[\frac{1}{\left(1 + \frac{DOB}{R}\tan\theta\right)^2}\right] - \frac{(B-1)}{3}\cdot\frac{DOB}{R}\left[\frac{1}{1 + \frac{DOB}{R}\tan\theta}\right] - \frac{(B-1)}{3}\cdot\frac{DOB}{R}\right\} \tag{35}$$

$$\frac{h}{DOB} = m\left\{\left[\frac{2(B+1)}{3}\cdot\frac{R}{DOB} - \frac{(B-1)}{3}\right]\left[\frac{\left(\frac{R}{DOB}\right)^2}{\left(\frac{R}{DOB}+\tan\theta\right)^2}\right] - \frac{(B-1)}{3}\left[\frac{\frac{R}{DOB}}{\frac{R}{DOB}+\tan\theta}\right] - \frac{1}{3}(B-1)\right\} \tag{36}$$

$$\frac{h}{CW^{1/3}} = m\left\{\left[\frac{2(B+1)}{3} - \frac{(B-1)}{3C}\cdot\frac{DOB}{W^{1/3}}\right]\left[\frac{1}{\left(1+\frac{1}{C}\cdot\frac{DOB}{W^{1/3}}\tan\theta\right)^2}\right] - \frac{(B-1)}{3C}\cdot\frac{DOB}{W^{1/3}}\left[\frac{1}{1+\frac{1}{C}\cdot\frac{DOB}{W^{1/3}}\tan\theta}\right] - \frac{(B-1)}{3C}\cdot\frac{DOB}{W^{1/3}}\right\} \tag{37}$$

$$\frac{h}{DOB} = m\left\{\left[\frac{2(B+1)}{3}\cdot\frac{CW^{1/3}}{DOB} - \frac{(B-1)}{3}\right]\left[\frac{\left(\frac{CW^{1/3}}{DOB}\right)^2}{\left(\frac{CW^{1/3}}{DOB}+\tan\theta\right)^2}\right] - \frac{(B-1)}{3}\left[\frac{\frac{CW^{1/3}}{DOB}}{\frac{CW^{1/3}}{DOB}+\tan\theta}\right] - \frac{1}{3}(B-1)\right\}. \tag{38}$$

The above equations are listed in <u>increasing</u> order of reliability (i.e., <u>decreasing</u> degree of scatter). Note again that the best relation (Eq. (38)) does not contain the measured cavity radius R. From the <u>actual</u> subsidence crater volumes, crater radii, crater depth, and Eq. (33),

the "shape factor" m can be found. The shape factor is plotted against the scaled DOB for each of the areas in Figures 16 through 19. A linear least-square fit (because of the large scatter in the data) was made to find the best relation between m and the scaled DOB. These relations are given in Table VII.

Note that as scaled DOB increases, the shape of the subsidence crater changes from conical, m = 3, to parabolic, m = 2.

By substituting Eqs. (39) through (42) (Table VII) into Eqs. (35) through (38), respectively, the subsidence-crater depths may be computed. These equations are plotted with the experimental points in Figures 20 through 23.

The scatter about the theoretical curves is similar to that for crater volumes. The discussion in Paragraph 4.3.1 regarding this scatter is also applicable for crater depths (i.e., bulking factors, tan θ, etc.).

TABLE VII

Shape Factor m/Scaled Burial Depth Relations

Area	Relation	Eq. No.
2A	$m = 7.45 - 0.013\left(DOB/W^{1/3}\right)$	(39)
3A	$= 4.18 - 0.0024\left(DOB/W^{1/3}\right)$	(40)
9A	$= 5.35 - 0.0060\left(DOB/W^{1/3}\right)$	(41)
9T	$= \left[5.00 - 0.0058\left(DOB/W^{1/3}\right)\right]^{*}$	(42)

*Least-squares method was not used to find the relation.

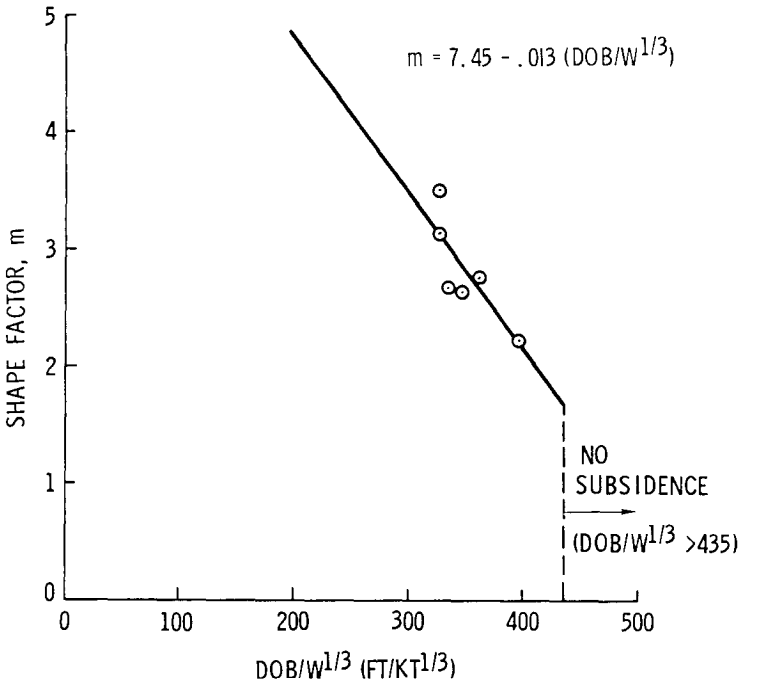

Figure 16. Shape factor vs scaled burial depth (Area 2 - alluvium)

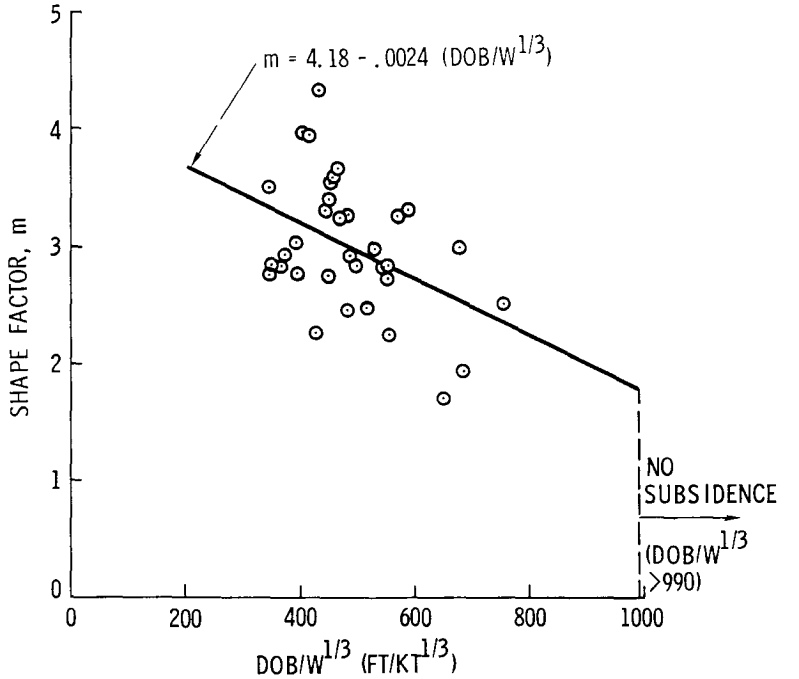

Figure 17. Shape factor vs scaled burial depth (Area 3 - alluvium)

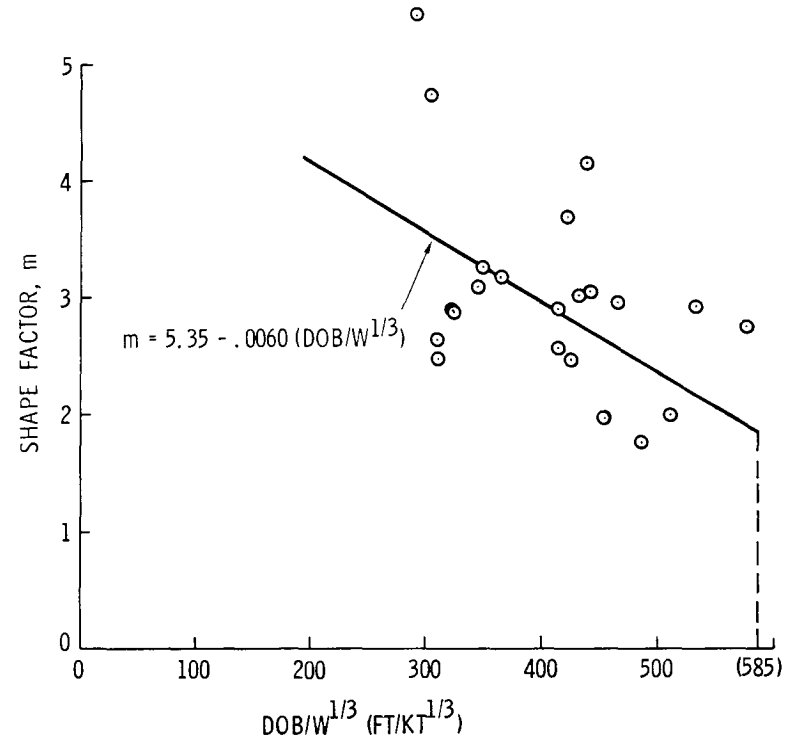

Figure 18. Shape factor vs scaled burial depth (Area 9 - alluvium)

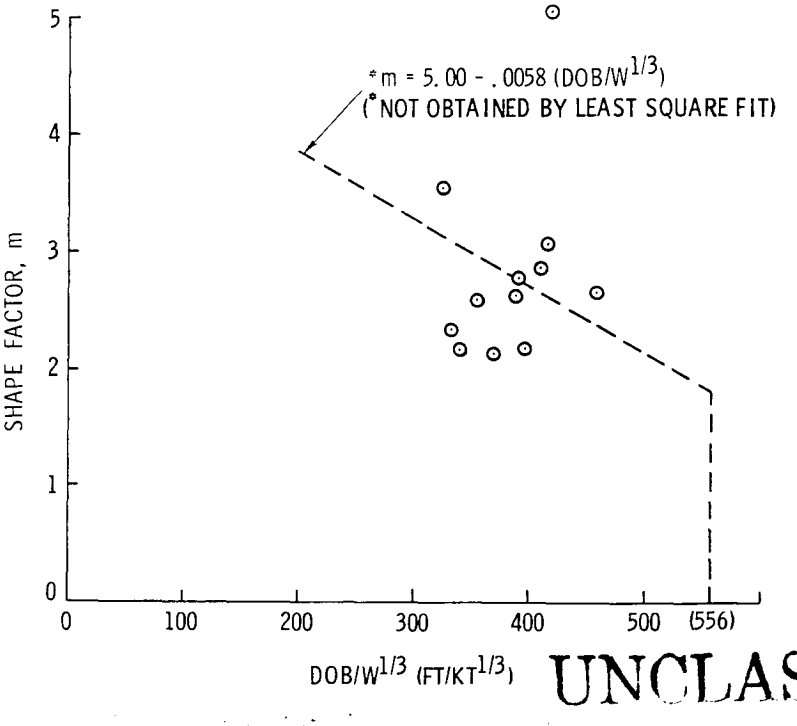

Figure 19. Shape factor vs scaled burial depth (Area 9 - tuff below alluvium)

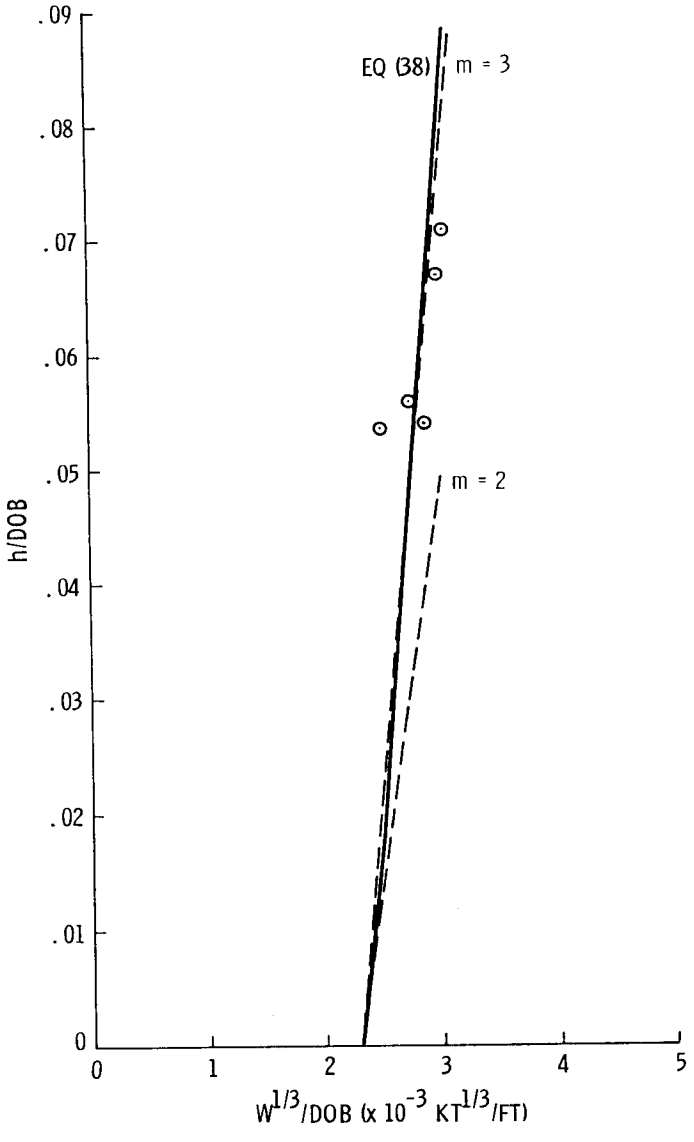

Figure 20. h/DOB vs $W^{1/3}/DOB$ (Area 2 - alluvium)

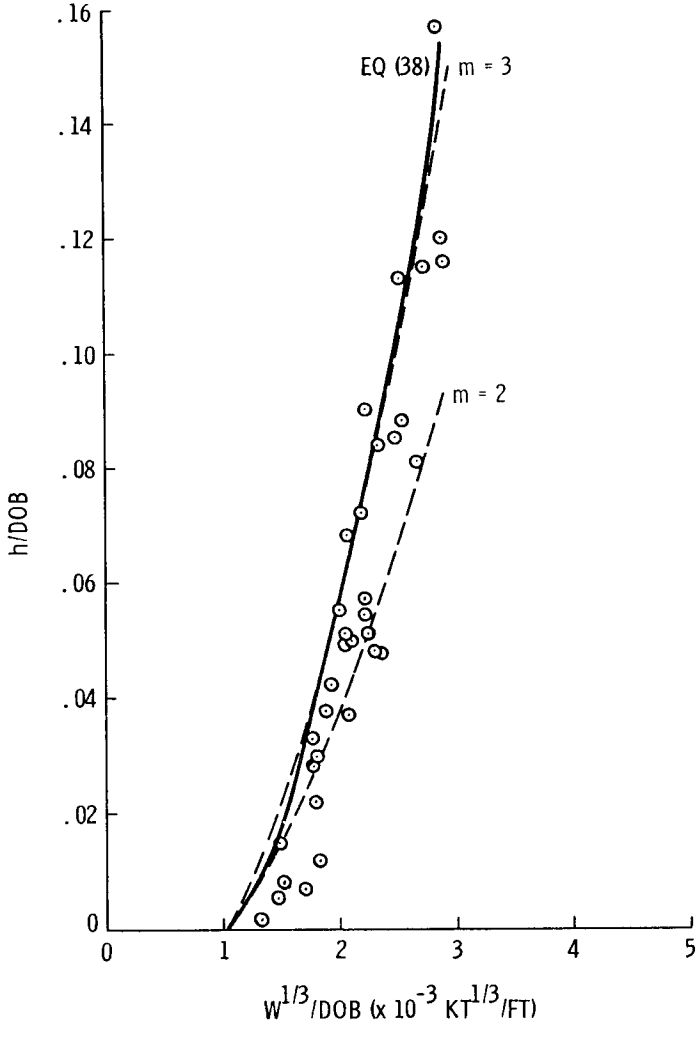

Figure 21. h/DOB vs $W^{1/3}/DOB$ (Area 3 - alluvium)

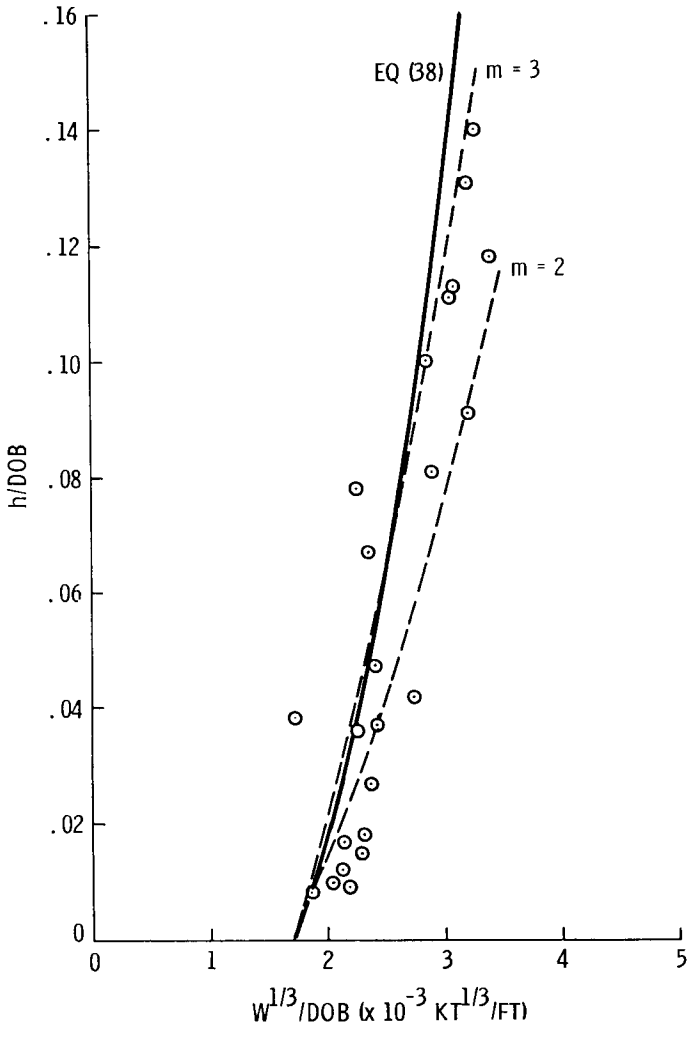

Figure 22. h/DOB vs $W^{1/3}/DOB$ (Area 9 - alluvium)

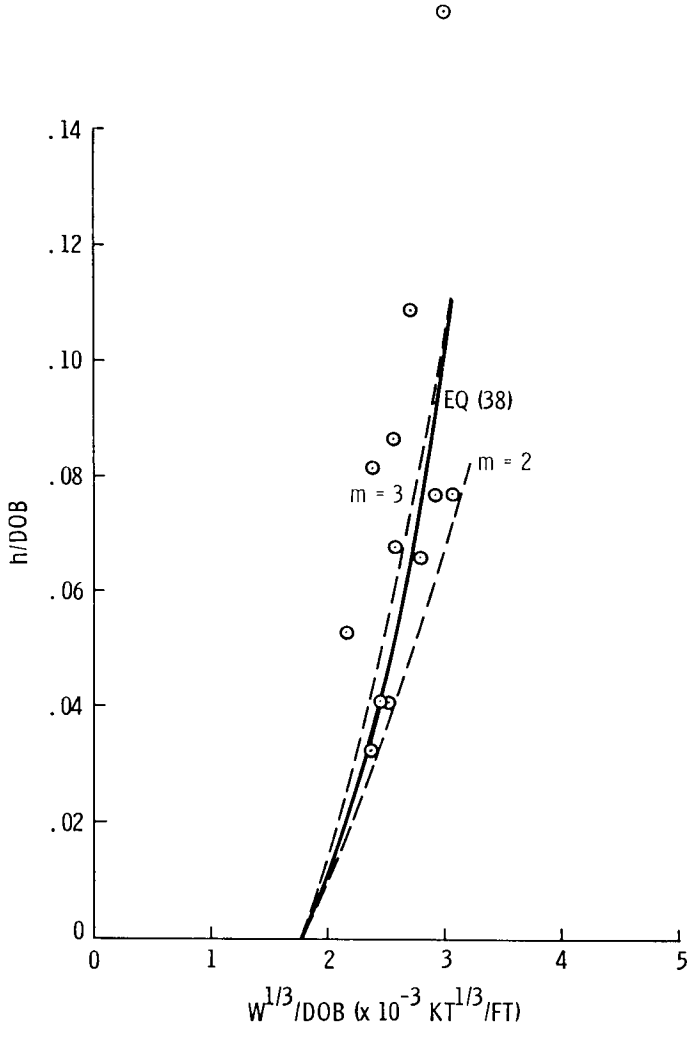

Figure 23. h/DOB vs $W^{1/3}/DOB$ (Area 9 - tuff below alluvium)

4.3.4 Collapse Times of Craters

Equation 43 deleted

The scatter in collapse-time data was greater than in crater dimensions. Various other dimensionless relations were attempted, but with less success. It was not even possible to find consistent relations for shots in alluvium in Areas 3 and 9 (which contained the most data). It was decided to try to determine the reason for the inconsistencies.

Shown in Figure 24a is a simplified sketch of the mass of material affected near the conclusion of cavity growth. Although Boardman, Rabb, and McArthur[3] assumed that the pressure when the cavity had reached its maximum size is equal to the overburden pressure, it can be shown that cavity pressure may be much larger than this value.

Placing the cylindrical soil mass above the cavity in equilibrium by equating the vertical forces to zero,

$$\int_0^{DOB} \pi R^2 w dz + \int_0^{DOB} (c + K\sigma_v \tan\phi)\, 2\pi R dz = p_1 \pi R^2, \qquad (44)$$

where

w = unit weight of soil ($w = \rho g$)

z = any distance between surface and burst depth

c = cohesion of soil

K = coefficient of lateral earth pressure

σ_v = vertical pressure in soil

σ_H = lateral pressure in soil

ϕ = angle of internal friction of soil

p_1 = cavity pressure at conclusion of growth,

and the remaining quantities have been previously defined. After substituting $\sigma_v = wz$, and solving,

$$p_1 = w(DOB) + K \tan \phi \cdot w(DOB)(DOB/R) + 2c(DOB/R). \qquad (45)$$

The first term on the right side is the overburden pressure, while the second and third terms represent the frictional and cohesive resisting forces, respectively. Since typical values of $K \tan \phi$ are of the order of unity, it can be seen that the frictional term is approximately (DOB/R) times larger than the overburden pressure ($w \cdot DOB$). For contained nuclear explosions, (DOB/R) is larger than about 5 (Paragraph 4.3.1). Therefore, even in the absence of cohesive strength (i.e., $c = 0$), cavity pressure may greatly exceed overburden pressure. The assumption of equivalence to overburden pressure is probably a lower limit on final cavity pressure.

As cavity pressure dissipates, the frictional and cohesive resisting forces reduce in value. When cavity pressure drops below overburden pressure, the frictional and cohesive forces change direction, to resist downward movement of the soil mass into the cavity (Figure 24b). For simplicity, a cylindrical mass will be assumed again, although the real failure surface is probably represented by the dotted lines in Figure 24b.

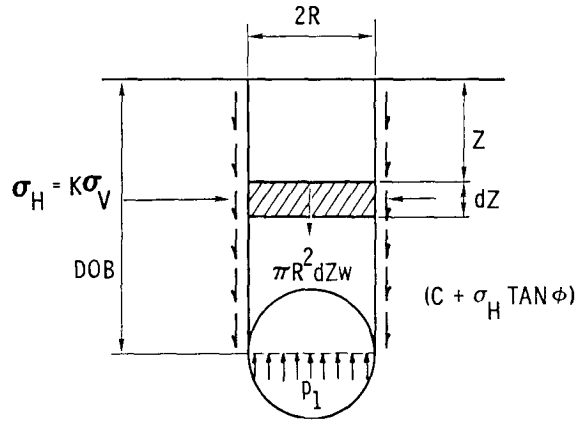

a.

Figure 24.

Forces on soil mass above cavity

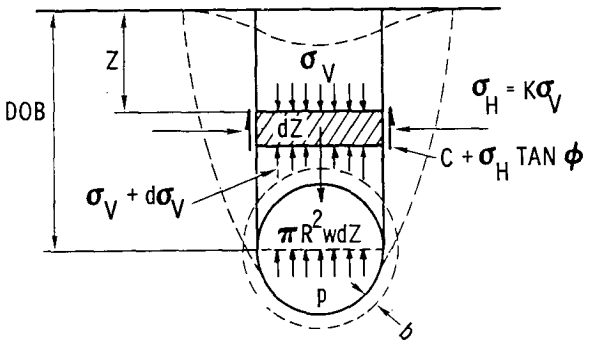

b.

It is assumed that collapse of material into the cavity will begin when vertical stress in the soil mass above the cavity reaches some "critical" value. This value may not be a constant, but will depend upon the size of the cavity. Assuming that the spherical shape of the cavity will resist "arching" forces to some degree, it would seem reasonable that collapse would begin when the stress in the wall of the cavity reaches a constant value S_f, that is a function of the material. If the cavity is approximated by a thin-walled sphere of thickness b, the value S_f can be found:

$$S_f \cdot 2\pi Rb \cong (\sigma_{vf} - p)\pi R^2 \qquad (46)$$

or

$$S_f = \frac{(\sigma_v - p)R}{2b}. \tag{47}$$

Stated in another way, collapse will begin when cavity pressure p has reduced to:

$$p_c = \sigma_v - \frac{2bS_f}{R}. \tag{48}$$

The pressure σ_v may be obtained from an approximate arching theory[23] that has been found to fairly represent field conditions. For equilibrium of the elemental soil mass in Figure 24b:

$$\pi R^2 w dz = \pi R^2(\sigma_v + d\sigma_v) - \pi R^2 \sigma_v + 2\pi R c dz + 2\pi R K \sigma_v \tan\phi \cdot dz. \tag{49}$$

After solving this differential equation subject to the boundary condition that $\sigma_v = 0$ at $z = 0$,

$$\sigma_v = \frac{R(w - 2c/R)}{2K \tan\phi}\left[1 - e^{-2K \tan\phi \cdot z/R}\right] \tag{50}$$

If this value of σ_v is substituted into Eq. (48), the cavity pressure at which collapse begins may be obtained.

$$p_f = \frac{R(w - 2c/R)}{2K \tan\phi}\left[1 - e^{-2K \tan\phi \cdot (DOB/R)}\right] - \frac{2bS_f}{R}. \tag{51}$$

Assuming adiabatic expansion of cavity gases through the voids of the surrounding medium (γ = gas constant),

$$p_1 V_1^{\gamma} = p_2 V_2^{\gamma}, \tag{52}$$

where p_1 and V_1 are the pressure and volume of the cavity at the conclusion of cavity growth, and p_2 and V_2 are the corresponding values for

the gases at a later time. If the adiabatic expansion is symmetrical about the cavity, Eq. (52) may be expressed:

$$p_1 V_1^{\gamma} = p_2\left[V_1 + n\left(V_2 - V_1\right)\right]^{\gamma}, \tag{53}$$

where n is the porosity of the medium.

The above equation may also be written as

$$\frac{V_2}{V_1} = \frac{1}{n}\left[\left(\frac{p_1}{p_2}\right)^{1/\gamma} - (1 - n)\right] = \frac{r^3}{R^3}, \tag{54}$$

where r is the radius to the extreme boundary of the expanding gases. Initial collapse will begin when $p_2 = p_f$. Also, p_f may be found from Eq. (51). For contained nuclear explosions [(DOB/R) $\gtrsim$ 5], Eq. (51) reduces to

$$p_f \simeq \frac{R(w - 2c/R)}{2K \tan \phi}. \tag{55}$$

As discussed earlier, the smallest probable value of p_1 is equal to the overburden pressure. Thus, the smallest value of p_1/p_f is

$$\frac{p_1}{p_f} = \frac{DOB}{R} \cdot \frac{w \cdot 2K \tan \phi}{(w - 2c/R)}. \tag{56}$$

The smallest value of this ratio results for a cohesionless soil (c = 0). Since 2K tan $\phi \approx 1$,

$$\frac{p_1}{p_f} > 5. \tag{57}$$

Using the polytropic gas constant, $\gamma = 4/3$ (Reference 3), and substituting into Eq. (51),

$$\frac{r_f^3}{R^3} \approx \frac{1}{n}\left(\frac{p_1}{p_f}\right)^{3/4}. \tag{58}$$

Assuming a typical value of porosity, say n = 30%, $r^3/R^3 > 11$. Thus

$$\frac{r_f}{R} > 2.2, \tag{59}$$

which means that the outer boundary of the expanding gas may be near the surface before collapse begins.

Theoretically, based upon the above approximations and assumptions, it may be possible to determine the time at which collapse is initiated (t_f). Assuming the validity of Darcy's Law for fluid flow through a porous medium (even though the gas is compressible),

$$v = -ki = -\frac{k}{\rho g} \cdot \frac{dp}{dr}, \tag{60}$$

where

v = flow velocity of gas at outer boundary (LT^{-1})

k = permeability of medium (LT^{-1})

$i = \frac{1}{\rho g} \cdot \frac{dp}{dr}$ = pressure gradient,

t_f may be calculated from the relation,

$$t_f = \int_R^{r_f} \frac{dr}{v} = -\int_R^{r_f} \frac{dr}{ki}. \tag{61}$$

The pressure gradient i may be computed from Eq. (54), if put in another form, i.e.,

$$p \cong p_1 \left(\frac{R^3}{nr^3}\right)^{\gamma}. \tag{62}$$

$$\frac{dp}{dr} = -\frac{3\gamma p_1 R^{3\gamma}}{n^{\gamma}} r^{(-3\gamma-1)}. \tag{63}$$

Substituting into Eq. (61) and solving,

$$t_f \approx \frac{\rho g n^{\gamma}}{3(3\gamma + 2)k\gamma p_1} \cdot \frac{r_f^{3\gamma+2}}{R^{3\gamma}} \tag{64}$$

or

$$t_f = K_1 \frac{r_f^{3\gamma+2}}{R^{3\gamma}}, \tag{65}$$

where

$$K_1 = \frac{\rho g n^{\gamma}}{3(3\gamma + 2)k\gamma p_1}.$$

Equation (65) gives the initial time of collapse in terms of the outer boundary r_f. Solving for r_f and then substituting into Eq. (62) gives

$$p_f = \frac{p_1 K_1^{3\gamma/3\gamma+2}}{n^{\gamma} t_f^{3\gamma/3\gamma+2}} \cdot R^{6\gamma/3\gamma+2}. \tag{66}$$

Equating this to p_f in Eq. (55),

$$K_2 \frac{R^{6\gamma/3\gamma+2}}{t_f^{3\gamma/3\gamma+2}} \approx \frac{R(w - 2c/R)}{2K \tan \phi}. \tag{67}$$

Assuming $\gamma = 4/3$ and no cohesion (Eq. (45)).

$$\left.\begin{aligned} t_f &\propto R^{1/2} p_1^{1/2} \cdot \propto R^{1/2} \mathrm{DOB}^{1/2} \\ t_f &\propto R \quad \text{(for most shots)} \end{aligned}\right\} \tag{68}$$

If the cohesion is very large, $t_f \rightarrow \infty$. Contrastingly, if ϕ is very small (little friction), $t_f \rightarrow 0$.

The preceding analysis indicates that collapse time is proportional to some power of the cavity radius (varying from $-\infty$ to $+\infty$), depending upon the strength properties of the medium. (The cohesion of materials at NTS varies from 0 to very large values.) This would account for the large scatter in the experimental data.

Although t_f is the time from termination of cavity growth to initial collapse, it is the major portion of the total collapse time, t_c. Cavity formation occurs in a fraction of a second,[19] while the time involved between initial collapse and subsidence of the surface is given approximately by

$$t' \cong \int_0^{DOB} \frac{dz}{v} = \int_0^{DOB} \frac{dz}{\sqrt{2g \cdot 2R}} = \frac{DOB}{2\sqrt{gR}}, \tag{69}$$

since the "drop" height is approximately the diameter of the cavity (neglecting bulking). This time would be about 10 seconds for a 1000-foot depth and a 100-foot cavity radius. This is a small fraction of the total collapse time.*

Since this approximate analysis indicated that collapse time was a function of cavity radius, least-square fits (Figures 25 through 28) were made to t_c versus W data (since W is a better indicator of cavity geometry than the measured R) for each of the areas. This scatter was slightly less than that obtained using the relation Eq. (4e), and a strong correlation was found for three of the four areas (contrasted to two areas for relation Eq. (4e)). These "best fit" equations are given in Table VIII.

*A collapse propagation velocity of 70 to 125 fps was recorded on a recent NTS test (Vulcan), which agrees with the above figures.[22]

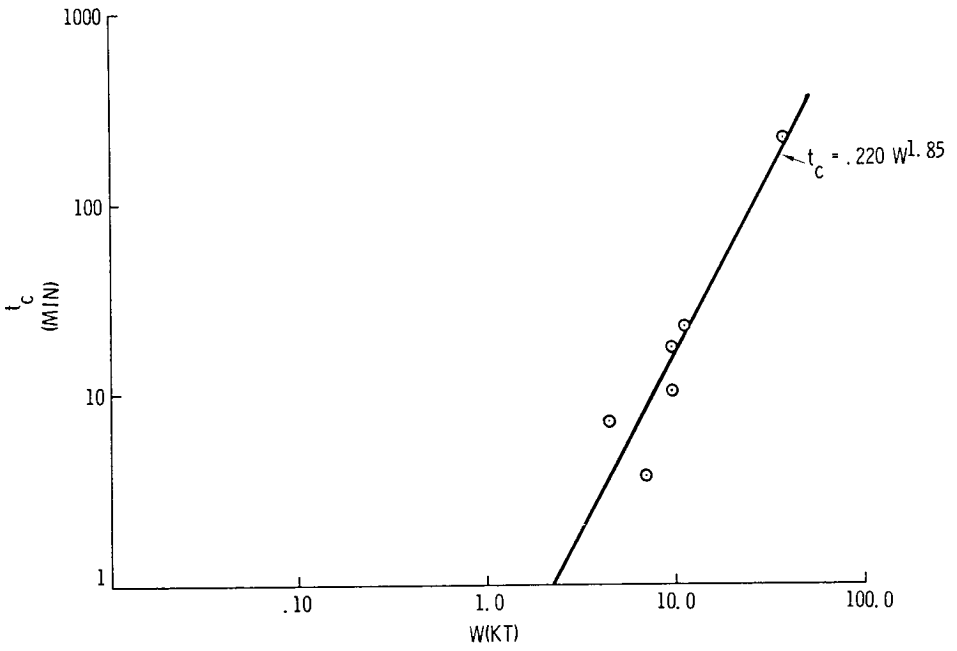

Figure 25. Collapse times vs yield
(Area 2 - alluvium)

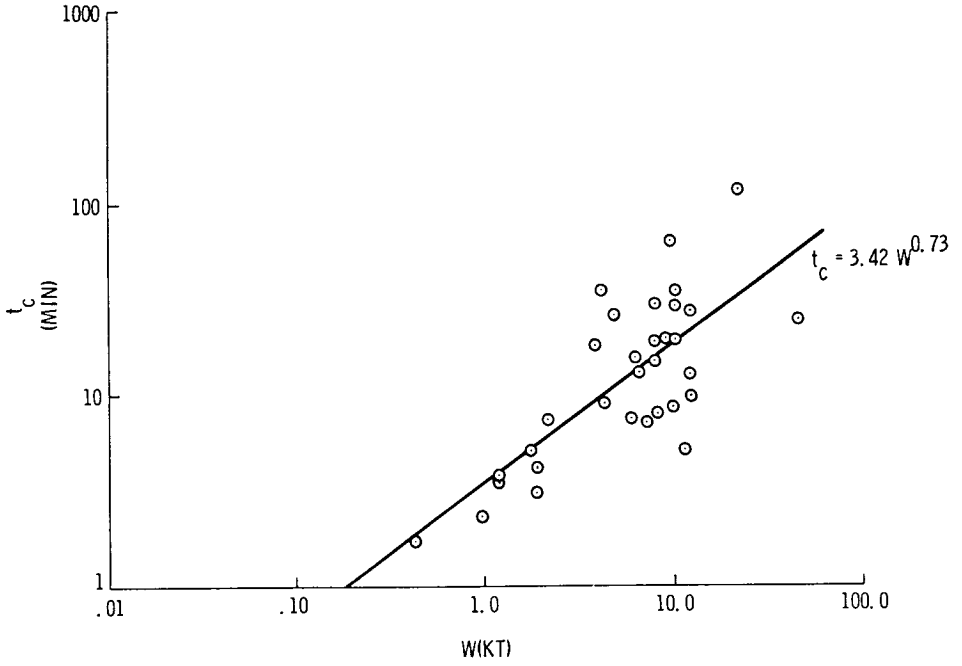

Figure 26. Collapse times vs yield
(Area 3 - alluvium)

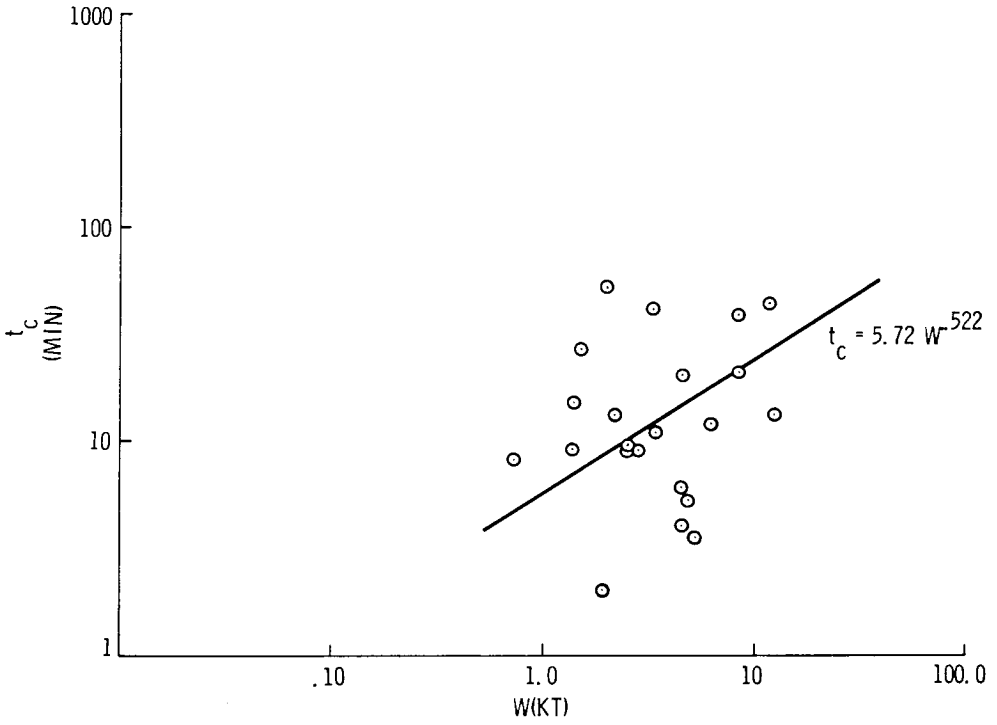

Figure 27. Collapse times vs yield (Area 9 - alluvium)

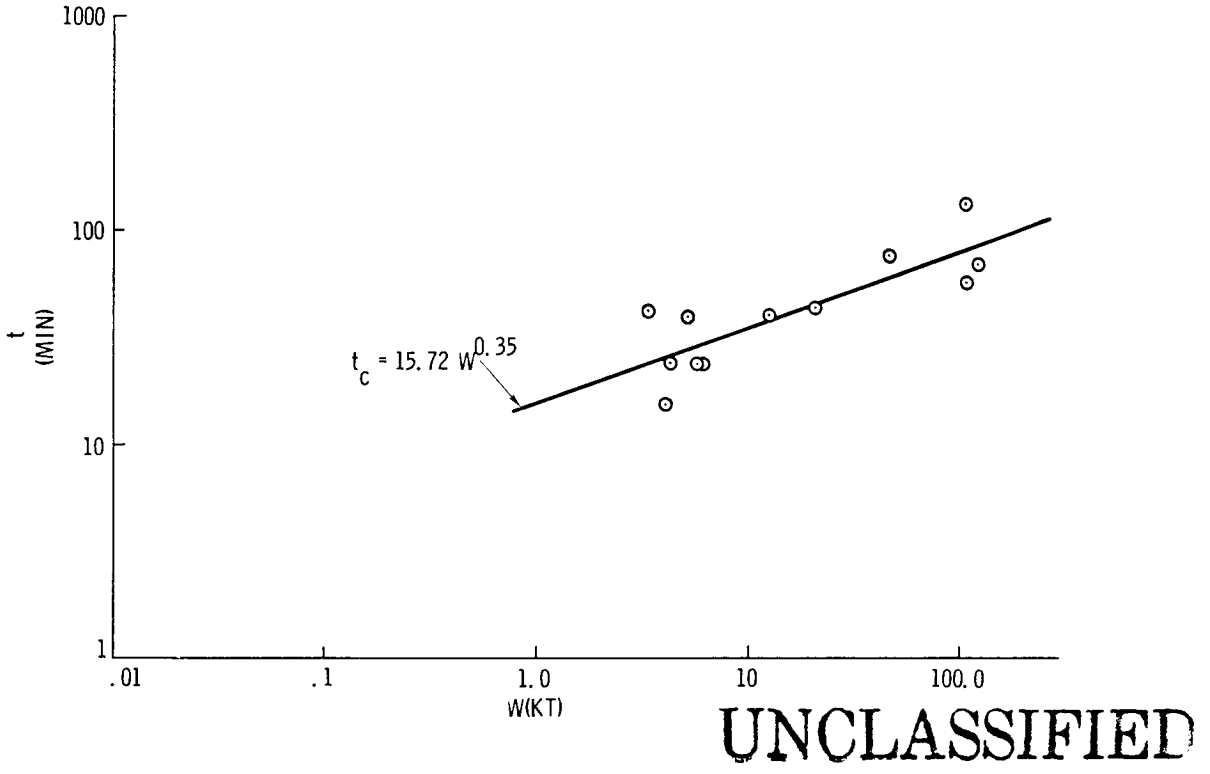

Figure 28. Collapse times vs yield (Area 9 - tuff below alluvium)

TABLE VIII

"Best Fit" Equations for Collapse Times of Subsidence Craters (t_c vs W)

Area	Relation*	Eq. No.
2A	$t_c = 0.220\ W^{1.85}$	(70)
3A	$= 3.42\ W^{0.73}$	(71)
9A	(too much scatter)	(72)
9T	$= 15.72\ W^{0.35}$	(73)

*t_c in minutes; W in kilotons.

The relation obtained by dimensional analysis,

$$t_c W^{1/2}/DOB^{5/2} = K_i\left(\frac{DOB}{W^{1/3}}\right)^{\alpha} \tag{74}$$

may be rewritten as

$$t_c = K_i \frac{DOB^{(5/2+\alpha)}}{W^{1/2+\alpha/3}}$$

or

$$t_c = K_i\left(\frac{DOB}{W^{1/3}}\right)^{5/2+\alpha} \cdot W^{+1/3}. \tag{75}$$

Since the burial depth was generally a constant times the cube root of the yield (i.e., $DOB \propto W^{1/3}$), Eq. (75) may be expressed as

$$t_c \simeq K_i' W^{+1/3}. \tag{76}$$

This is similar in form to the equation obtained by the approximate analysis (Table VIII), and probably accounts for the scatter in the fits being similar.

4.4 Determination of Yield from Crater Dimensions and Collapse Times

In the previous sections, an attempt has been made to predict, by means of a bulking theory, the cavity size, dimensions of the subsidence crater (volume, radius, and depth), and collapse time for a given yield and DOB. It is believed that the scatter of the experimental data about the theoretical curves could be greatly reduced if correlations could be made with the physical and mechanical properties of the geologic materials, which are presently unknown. In the absence of these relations, Eqs. (17), (23), and (38) may be used to predict with a fair degree of reliability the crater volume, radius, and depth, respectively. Because of the numerous factors affecting collapse time, empirical equations must be used to predict this parameter.

Presently, quite sophisticated techniques are employed to determine yield (Paragraph 3.1). A range is normally given for the yield, usually within ±10 percent of the mean value. It would be extremely valuable if simpler and less costly procedures of determining yield could be found. In this regard, the curves in Figures 8 through 11, 12 through 15, 20 through 23, and 25 through 28 could be used to calculate the yield. However, the accuracy of predicting the yield from any of these curves is quite low. Possibly accuracy could be improved by combining the various curves.

A Multiple Regression Analysis was made on the various parameters of the subsidence craters; i.e., volume, depth, radius, and collapse times. It was found that empirical equations (Table IX) can be used to predict the yield in Areas 3 and 9 (both alluvium) at NTS. Not enough data were available to make a statistical study in other areas.

As would be expected, if no subsidence results (i.e., $V_s = a = h = 0$), the empirical equations give values of $(W^{1/3}/DOB)$ that are very similar to the critical values shown in Figures 9b, 10b, 13, 14, 21, and 22. It is also noteworthy that the parameters included in the empirical equations differ for the two areas.

TABLE IX

Empirical Equations for Determining Yield

Area	Relation*	Eq. No.
3A	$W^{1/3}/DOB = 0.00107 + 86.7\left(\frac{V_s}{DOB^3}\right) + 0.0025\left(\frac{a}{DOB}\right) + 0.0065\left(\frac{h}{DOB}\right)$	(77)
9A	$= 0.00209 + 9.04(10)^{9}\left(\frac{V_s}{DOB^3}\right)^2 - 9.52(10)^{15}\left(\frac{V_s}{DOB^3}\right)^3 + 3.49(10)^{-6}\left(\frac{t_c^3}{DOB}\right)$	(78)

*W in kilotons; V_s in thousands of cubic yards; a, h, and DOB in feet.

Figures 29 and 30 show the plots scaled from the measured yields versus the values obtained from Eqs. (77) and (78), respectively. Note that approximately 50 percent of the points lie within W ± 0.10W, and about 80 percent of the values are within the range W ± 0.20W. Therefore, the use of empirical equations for predicting yield from subsidence crater parameters is almost as accurate as the more sophisticated methods presently being used. This accuracy could be further improved with a knowledge of the physical and mechanical properties of the geologic material.

Although information was insufficient to permit regression analyses to be made in other areas, it appears that yields in Area 2A could be approximated by Eq. (78).

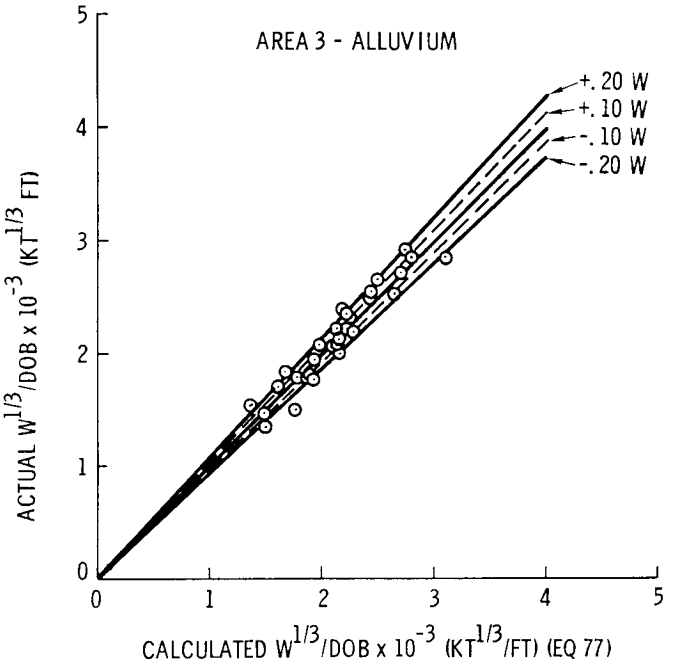

Figure 29. Comparison of "true" yield with yield obtained from Eq. (77)

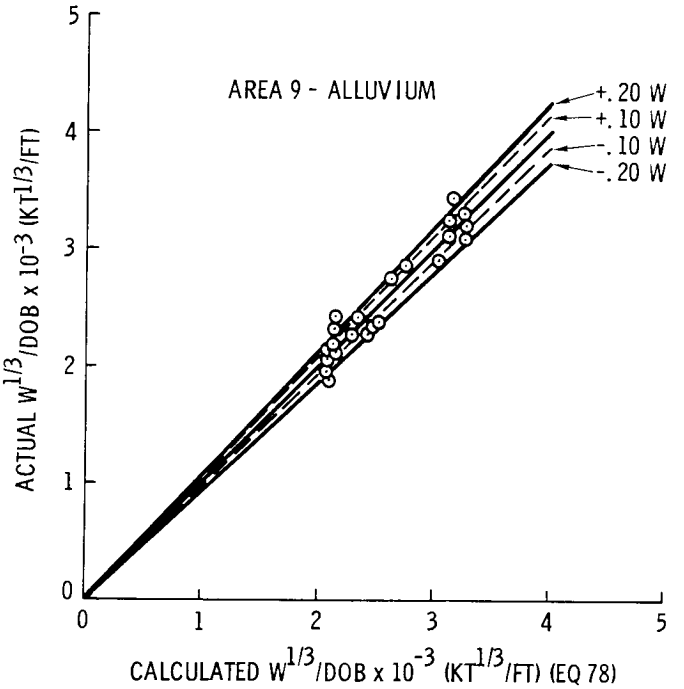

CHAPTER V

Conclusions and Recommendations

From the results of tests in similar geologic materials (at the alluvium-tuff interface), it was found that cavity radius scales as the 1/3 power of the yield. The effect of DOB on cavity size was not determinable, since larger yields were usually accompanied by larger DOB's. The physical properties of the medium appeared to be very important in determining the size of the cavity.

Studies of the volumes of subsidence craters indicated that measured cavity radius is not always a true indicator of cavity geometry. The most consistent correlations were found to exist between subsidence crater values and scaled burial depth ($DOB/W^{1/3}$). Differences do exist in the various NTS test areas; e.g., for the same scaled DOB's, the volumes of subsidence craters in Area 3 were almost twice as large as those in Area 9. This variation is probably due to the characteristics of the overlying material. A "bulking" theory is developed to predict the volumes of subsidence craters from the yield W and DOB.

The depths and radii of subsidence craters depend not only on crater volumes, but also upon scaled DOB's. Both the depth and radius decrease with increasing scaled DOB. A shape factor (dependent on the scaled DOB) is found that relates crater depth to crater volume. Also, the angle θ that the failure surface makes with the vertical depends on the scaled DOB.

Analysis of collapse times indicates that these times depend to a great extent on the strength properties of the medium, and are therefore subject to large variations.

REFERENCES

1. Bennett, W. P., Anderson, A. L., and Smith, B. L., Cavity Definition, Radiation and Temperature Distributions Resulting from the Logan Event, UCRL 6240, Contract No. W-7405-eng-48, Lawrence Radiation Laboratory, December 1960, 54 pages.

2. Berry, Richard H., Major Controls of Bulking Factors of Chimney Rubble, (Draft) NVO-1163-37, Roland F. Beers, Inc., Alexandria, Virginia, July 22, 1966, 26 pages (classified).

3. Boardman, Charles R., Rabb, David D., and McArthur, Richard D., Characteristic Effects of Contained Nuclear Explosions for Evaluation of Mining Applications, UCRL-7350, Contract No. W-7405-eng-48, Lawrence Radiation Laboratory, May 3, 1963, 47 pages.

4. Brownlee, Robert R., The Hydrodynamic Yields of Underground Shots, December 1961-June 1963, Los Alamos Scientific Lab, LAMS-2914, June 1963 (classified).

5. Carroll, R. D., Preliminary Interpretation of Geophysical Logs from the U3ao Site, Nevada Test Site, Technical Letter: Yucca-8, Supplement 1, USGS, January 31, 1962, 3 pages.

6. Carroll, R. D., Preliminary Interpretation of Geophysical Logs from the U3ao Site, Nevada Test Site, Technical Letter: Yucca-7, Supplement 1, January 31, 1962, 4 pages.

7. Chabai, A. J., Scaling Dimensions of Craters Produced by Buried Explosions, Research Report, SC-RR-65-70, TID-4500 (37th Edition) Sandia Corporation, February 1965, 53 pages.

8. Cherry, J. T., Computer Calculations of Explosion - Produced Craters, UCRL-14998 (Preprint), Lawrence Radiation Laboratory, July 14, 1966, 51 pages.

9. Cole, T. H. and Williams, W. P., The Lithology of the U3-ax Drill Hole Site, Area 3, Nevada Test Site, Technical Letter: Yucca-16, USGS, March 26, 1962, 2 pages.

10. Davis, Dale S., Nomography and Empirical Equations, Reinhold Publishing Corp., 1955, 236 pages.

11. Graves, Alvin C., Summary of Yield Data Operation Nougat, Los Alamos Scientific Laboratory, LA-3145-MS, August 1964, 4 pages (classified).

12. Graves, Alvin C., Summary of Yield Data Operation Niblick, Los Alamos Scientific Laboratory, LA-3207-MS, August 1964, 4 pages (classified).

13. Graves, Alvin C., Summary of Yield Data Operation Storax, Los Alamos Scientific Laboratory, LA-3146-MS, August 1964, 4 pages (classified).

14. Graves, Alvin C., Summary of Yield Data Operation Whetstone, Los Alamos Scientific Laboratory, LA-3390-MS, July 1965, 4 pages (classified).

15. Hankins, Dorris M., Seismic Yield Estimate of LASL Shots During Operations Nougat, Storax, and Niblick, SC-WD-65-336, Sandia Corporation, July 1965, 28 pages (classified).

16. Knox, Joseph B. and Terhune, Robert W., Cratering Physics Concepts of Ground Surface Motion, UOPKA 63-18, Lawrence Radiation Laboratory, October 1963.

17. Knox, J. B. and Terhune, R. W., "Calculation of Explosion-Produced Craters," Proceedings of the Third Plowshare Symposium, Engineering with Nuclear Explosives, April 21-23, 1964, pp. 75-98.

18. Lindgren, B. W., Statistical Theory, The MacMillan Company, 1962, 427 pages.

19. Nuckolls, John H., "A Computer Calculation of Rainier (The First 100 Milliseconds," Proceedings of the Second Plowshare Symposium Part I: Phenomenology of Underground Nuclear Explosives, UCRL-5675, May 13-15, 1959, pp. 120-134.

20. Pelsor, G. T., "Cavity Formation," Proceedings of the Second Plowshare Symposium, Part I: Phenomenology of Underground Nuclear Explosions, UCRL-5675, May 13-15, 1959, pp. 114-119.

21. Rogich, Donald and Rich, Charles, A Statistical Analysis of Post-Shot Data Pertaining to Cavity Radii, NVO-1163-61, Roland F. Beers, Inc., 813 North Royal Street, Alexandria, Virginia, March 23, 1966, 82 pages (classified).

22. Roland F. Beers, Inc., An Empirical Data Summary of Underground Nuclear Events, NVO-1163-5, Alexandria, Virginia, April 8, 1966, 43 pages (classified).

23. Sisemore, Clyde J., Collapse Slifers on the Vulcan Event, Lawrence Radiation Laboratory, UOPKB 66-85, July 27, 1966, 5 pages.

24. Terzaghi, Karl, Theoretical Soil Mechanics, John Wiley and Sons, Inc., 1943, 510 pages.

25. Vortman, L. J., Craters by Collapse of Cavities Formed by Underground Nuclear Explosions, SC-4734(WD), Sandia Corporation, RS 3423/1096, October 1962, 54 pages (classified).

26. Williams, W. P., The Lithology of the U3ag and U3ag-3 Drill Hole Sites, Area 3, Nevada Test Site, Technical Letter: Yucca-7, USGS, January 16, 1962, 4 pages.

27. Williams, W. P., The Lithology of the U3ao Site, Area 3, Nevada Test Site, Technical Letter: Yucca-7, USGS, January 16, 1962, 4 pages.

[redacted]

UNCLASSIFIED

DISTRIBUTION:

Maj. Gen. Edward B. Giller, USAF
Assistant General Manager for
Military Application
U.S. Atomic Energy Commission
Washington, D.C. 20545

U.S. Atomic Energy Commission
Division of Technical Information
Reports Section
Headquarters Library, G-017
Washington, D.C. 20545
For delivery to:
Dept. of Nuclear Explosives
For: J. S. Kelly, Director (25)
Richard Hamburger (1)
William Oakley (1)
Div. of Health and Safety
For: G. M. Dunning (1)

U.S. Atomic Energy Commission
San Francisco Operations Office
2111 Bancroft Way
Berkeley, California 94704

U.S. Atomic Energy Commission
Nevada Operations Office
P.O. Box 14100
Las Vegas, Nevada 89114
Attn: Document Control Clerk
For: J. E. Reeves (2)
G. B. Maxey,
Consultant (1)
T. F. Thompson,
Consultant (1)
Fred Houser,
USGS (1)

U.S. Atomic Energy Commission
Sandia Area Office
P.O. Box 5400
Albuquerque, New Mexico 87115
Attn: P. W. Ager

U.S. Atomic Energy Commission
Albuquerque Operations Office
P.O. Box 5400
Attn: T-A Station
Albuquerque, New Mexico 87115

University of Illinois
Civil Engineering Department
111 Talbot Laboratory
Urbana, Illinois 61801
Attn: Joshua L. Meritt, Jr.
For: N. M. Newmark

Commanding Officer
U.S. Army Ballistic Research
Laboratories
Attn: Security Officer
Aberdeen Proving Ground
Maryland 21005
For: C. W. Lampson (1)
J. J. Meszaros (1)

Chief
Administrative Services Branch
Defense Atomic Support Agency
Washington, D.C. 20305

Los Alamos Scientific Laboratory
P.O. Box 1663
Los Alamos, New Mexico 87544
Attn: Report Librarian
For: J. C. Mark
W. E. Ogle
R. W. Newman

University of California
Lawrence Radiation Laboratory
P.O. Box 808
Livermore, California 94550
Attn: Technical Information
Division
For: D. Sewell (1)
G. C. Werth (1)
G. H. Higgins (10)
M. D. Nordyke (1)
W. Slazak, NCG (1)
Library:
M. M. May, Director (1)
A. C. Haussman,
Assoc. Director (1)

Commanding Officer
Edgewood Arsenal
Attn: Classified Document
Control Officer
Edgewood Arsenal, Maryland
21010

U.S. Atomic Energy Commission
Oak Ridge Operations Office
P.O. Box E
Oak Ridge, Tennessee 37830

UNCLASSIFIED

[redacted]

DISTRIBUTION (Cont):

Director
Air Force Weapons Laboratory
(WLIL, E. Lou Bowman)
Kirtland Air Force Base,
New Mexico 87117

Director
Attn: Mr. Johnny S. Taylor
Security Officer
USAE Waterways Experiment Station
P.O. Box 631
Vicksburg, Mississippi 39181

Commander, FC DASA
Attn: Brig. Gen. W. E. Gernert
Deputy Commander, Weapons and Training
Sandia Base
Albuquerque, New Mexico 87115

U.S. Geological Survey
Building 25, Federal Center
Denver, Colorado 80225
Attn: William S. Twenhofel

J. A. Hornbeck, 1
J. W. Weihe, 1710
C. R. Mehl, 5230
J. D. Shreve, Jr., 5271
R. A. Bice, 7000
L. E. Hollingsworth, 7200
T. B. Cook, Jr., 8000
G. A. Fowler, 9000
B. F. Murphey, 9100
C. D. Broyles, 9110
L. J. Vortman, 9111
M. L. Merritt, 9111 (2)
G. E. Hansche, 9120
H. E. Viney, 9130
R. K. Petersen, 9132
B. F. Hefley, 8232 (5)
J. G. Marsh, 3414
B. R. Allen, 3421
L. C. Baldwin, 3412
C. H. Sproul, 3428-2 (30)